Supporting Information for

A Molecular Strategy for Raman Enhancement

Ying-Fan Tan[1]†, Yangbo Zhang[1]†, Xiong Wang[2], Ning Zhou[1], Qingyun Wan[1]*

[1]Department of Chemistry, The Chinese University of Hong Kong, Hong Kong, China.

[2]Department of Physics, The University of Hong Kong, Pokfulam Road, Hong Kong, China.

*Corresponding author: qingyunwan@cuhk.edu.hk

†These authors contributed equally to this work.

Table of Content

1. Experimental Section

Raman spectroscopy was performed using an XploRA Plus Raman/PL spectrometer (Horiba Scientific) with the following parameters (unless otherwise specified): excitation wavelength = 532 nm, laser power = 18 μW, 100 × objective, slit width = 50 μm, pinhole = 100 μm, exposure time = 10 s and laser spot area = 44.2 μm^2. Raman mapping was performed using an inVia™ confocal Raman microscope (Renishaw) with the following parameters: excitation wavelength = 532 nm, laser power = 5 μW, 100 × objective, exposure time = 0.1 s. ^{1}H-NMR spectra were acquired on a Bruker AVANCE III HD 500 NMR spectrometer. UV-vis spectra of solution-state sample was conducted using a Shimadzu UV3600 Plus UV/VIS/NIR spectrophotometer. Single-crystal X-ray diffraction data were collected on a Bruker D8 Venture X-Ray diffractometer. Current-voltage (I-V) characteristics were measured using a KEITHLEY 4200-SCS semiconductor parameter analyzer. Reflectance spectra were recorded with a home-made measurement system, where the output incident light is filtered by an optical bandpass filter, and the filtered light is relatively pure of specific wavelength, which is reflected into the confocal microscopic system by a beam splitter as the incident light. Newton EM CCD from ANDOR company is used to record the spectrum and the image.

The following materials were used as received:

Tetrabutylammonium bis(1,3-dithiole-2-thione-4,5-dithiolato)nickel(III) and bis(tetrabutylammonium) bis(1,3-dithiole-2-thione-4,5-dithiolato)palladium(II) (TCI) Bis(tetrabutylammonium) bis(1,3-dithiole-2-thione-4,5-dithiolato)zinc, rhodamine 6G, and rhodamine 19 perchlorate (Macklin). Dimethyl malonate (Energy Chemical). Silver conductive paint (Electrolube).

Solvents: Acetonitrile (ACS grade), methanol (ACS grade), ethanol (ACS grade), diethyl ether (2000 ppm water, stabilized with BHT, ACS grade), and dichloromethane (HPLC grade) (RCI Labscan, Thailand). *n*-Hexane (95%, ACS grade, Duksan, Korea). DMSO-d_6 (J&K Scientific). PBS buffer PH 7.4 (Servicebio). Deionized water was obtained

using a Thermo Scientific Smart2Pure 6 UV purification system.

Raman Spectroscopy Measurement shown in **Figure 3-4**: A stock acetonitrile solution of **R19**/R6G and $[M(dmit)_2]^{n-}$ complex was mixed in a 1:1 volume ratio to achieve the desired concentration. A 5 μL aliquot of the mixed solution was drop-cast onto a silicon wafer and allowed to dry under ambient conditions until complete solvent evaporation. Raman spectra were acquired from approximately 20 different sites per sample.

^{1}H-NMR Spectroscopy shown in **Figure 5**: **M-1/2** crystals or **R19**/**R6G** powder were dissolved in DMSO-d_6 at a concentration of 7.2×10^{-3} M for NMR analysis.

Raman Spectroscopy Measurement shown in **Figure 6**: **R6G** was dissolved in PBS buffer and [**Ni**] was dissolved in acetonitrile. Two kinds of solution were mixed in a 95:5 volume ratio to achieve the desired concentration. A 5 μL aliquot of the mixed solution was drop-cast onto a silicon wafer and allowed to dry under ambient conditions until complete solvent evaporation. Raman spectra were acquired from 20 different sites.

Electrical Transport Measurements: Two-probe DC conductivity measurements were performed on **M-1/2** single crystals. Due to their high intrinsic resistance, contact resistance was assumed negligible. Electrical contacts were established using gold wires (20 μm diameter) adhered with silver conductive paint or carbon paste.

Ni-1: A solution of tetrabutylammonium bis(1,3-dithiole-2-thione-4,5-dithiolato)nickel(III) (3.5 mg) in acetonitrile (3 mL) was mixed with a solution of rhodamine 19 perchlorate (26 mg) in ethanol (6 mL). The mixture was stored in the dark under static conditions. After one-week, elongated needle-like green crystals formed (1.2 mg, yield: 28%), suitable for spectroscopic and crystallographic analysis.

^{1}H-NMR (500 MHz, DMSO-d_6) δ 8.13 (br, 1H), 7.83 (br, 1H), 7.77 (br, 1H), 7.36 (br, 1H), 6.66 (s, 2H), 6.59 (s, 2H), 3.46

– 3.39 (m, 4H), 2.07 (s, 6H), 1.25 (br, 6H).

Pd-1: A solution of bis(1,3-dithiole-2-thione-4,5-dithiolato)palladium(II) (9.9 mg) in acetonitrile (3 mL) was mixed with a solution of rhodamine 19 perchlorate (10.4 mg) in ethanol (3 mL). The mixture was stored in the dark under static conditions, yielding elongated needle-like green crystals after four days (5.2 mg, yield: 39%).

^{1}H-NMR (500 MHz, DMSO-d_6) δ 13.01 (s, 1H), 8.21 (d, *J* = 8.2 Hz, 1H), 7.85 (t, *J* = 7.5 Hz, 1H), 7.79 (t, *J* = 7.6 Hz, 1H), 7.60 (br, 2H), 7.40 (d, *J* = 7.8 Hz, 1H), 6.88 (s, 2H), 6.76 (s, 2H), 3.49 – 3.44 (m, 4H), 2.08 (s, 6H), 1.25 (t, *J* = 7.1 Hz, 6H).

Zn-1: A solution of bis(tetrabutylammonium) bis(1,3-dithiole-2-thione-4,5-dithiolato)zinc (3 mg) in methanol (2 mL) was mixed with a solution of rhodamine 19 perchlorate (3.3 mg) in methanol (2 mL). Slow evaporation at 2 °C in the dark afforded large cubic green crystals after four days (0.8 mg, yield: 35%).

^{1}H-NMR (500 MHz, DMSO-d_6) δ 13.02 (s, 1H), 8.20 (br, 1H), 7.85 (t, J = 7.6 Hz, 1H), 7.79 (t, J = 7.5 Hz, 1H), 7.65 (br, 2H), 7.40 (d, J = 5.8 Hz, 1H), 6.87 (s, 2H), 6.76 (s, 2H), 3.45 (br, 4H), 3.18 – 3.14 (m, 8H), 2.07 (s, 6H), 1.57 (p, J = 8.0 Hz, 8H), 1.35 – 1.28 (m, 8H), 1.25 (t, J = 7.1 Hz, 6H), 0.93 (t, J = 7.3 Hz, 12H).

Ni-2: A solution of tetrabutylammonium bis(1,3-dithiole-2-thione-4,5-dithiolato)nickel(III) (3 mg) in acetonitrile (3 mL) was mixed with a solution of rhodamine 6G (2.1 mg) in acetonitrile (2 mL). The mixture was stored in the dark under static conditions, yielding elongated needle-like green crystals within one day (1.3 mg, yield: 34%).

^{1}H-NMR (500 MHz, DMSO-d_6) δ 8.23 (d, *J* = 7.3 Hz, 1H), 7.93 (br, 1H), 7.86 (br, 1H), 7.60 (br, 3H), 6.86 (s, 2H), 6.79 (s, 2H), 3.94 (br, 2H), 3.59 (br, 4H), 2.19 (s, 6H), 1.29 (br, 6H), 0.84 (t, *J* = 6.5 Hz, 3H).

Pd-2: A solution of bis(tetrabutylammonium) bis(1,3-dithiole-2-thione-4,5-dithiolato)palladium(II) (5 mg) in acetonitrile (3 mL) was mixed with a solution of rhodamine 6G (4.9 mg) in acetonitrile (2 mL). The mixture was stored in the dark under static conditions, yielding elongated plate-like green crystals within one day (3.2 mg, yield: 45%).

^{1}H-NMR (500 MHz, DMSO-d_6) δ 8.24 (d, *J* = 7.8 Hz, 1H), 7.90 (t, *J* = 7.4 Hz, 1H), 7.83 (t, *J* = 7.7 Hz, 1H), 7.70 (t, *J* = 6.0 Hz, 2H), 7.47 (d, *J* = 7.5 Hz, 1H), 6.94 (s, 2H), 6.80 (s, 2H), 3.94 (q, *J* = 7.1 Hz, 2H), 3.49 (p, *J* = 7.2 Hz, 4H), 2.09 (s, 6H), 1.26 (t, *J* = 7.1 Hz, 6H), 0.84 (t, *J* = 7.1 Hz, 3H).

Zn-2: A solution of bis(tetrabutylammonium) bis(1,3-dithiole-2-thione-4,5-dithiolato)zinc (5 mg) in acetonitrile (1 mL) was layered with a solution of rhodamine 6G (5.1 mg) in acetonitrile/water (1:1 v/v, 2 mL). Slow evaporation at 2 °C yielded elongated green crystals within one day (4.2 mg, yield: 69%).

^{1}H-NMR (500 MHz, DMSO-d_6) δ 8.24 (d, *J* = 7.9 Hz, 1H), 7.90 (t, *J* = 7.5 Hz, 1H), 7.83 (t, *J* = 7.7 Hz, 1H), 7.70 (br, 2H), 7.47 (d, *J* = 7.6 Hz, 1H), 6.94 (s, 2H), 6.80 (s, 2H), 3.94 (q, *J* = 7.2 Hz, 2H), 3.51 – 3.47 (m, 4H), 3.19 – 3.13 (m, 8H), 2.09 (s, 6H), 1.57 (p, *J* = 7.9 Hz, 8H), 1.35 – 1.28 (m, 8H), 1.26 (t, *J* = 7.2 Hz, 6H), 0.93 (t, *J* = 7.3 Hz, 12H), 0.84 (t, *J* = 7.1 Hz, 3H).

Ni: A solution of tetrabutylammonium bis(1,3-dithiole-2-thione-4,5-dithiolato)nickel(III) (4 mg) in acetonitrile (2 mL) was subjected to vapor diffusion of diethyl ether, yielding elongated green crystals (1.7 mg, yield: 43%).

Pd: Commercially obtained bis(tetrabutylammonium) bis(1,3-dithiole-2-thione-4,5-dithiolato)palladium(II) (purple needle-like crystals) was used directly for Raman spectroscopy.

Zn: A solution of bis(1,3-dithiole-2-thione-4,5-dithiolato)zinc (5 mg) in dichloromethane (1 mL) was layered with hexane (1 mL). After 12 h, red plate crystals formed (2.6 mg, yield: 52%).

1: A solution of rhodamine 19 perchlorate (2 mg) in acetonitrile (0.7 mL) was subjected to vapor diffusion of diethyl ether, yielding red crystals after 12 h (0.7 mg, yield: 35%).

^{1}H-NMR (500 MHz, DMSO-d_6) δ 13.03 (s, 1H), 8.23 (d, *J* = 7.9 Hz, 1H), 7.86 (t, *J* = 7.5 Hz, 1H), 7.80 (t, *J* = 7.6 Hz, 1H), 7.68 (br, 2H), 7.42 (d, *J* = 7.5 Hz, 1H), 6.92 (s, 2H), 6.80 (s, 2H), 3.48 (p, *J* = 7.1 Hz, 4H), 2.09 (s, 6H), 1.26 (t, *J* = 7.2 Hz, 6H).

2: A solution of rhodamine 6G (7 mg) in dichloromethane (2 mL) was layered with hexane (1 mL). After several days, red plate crystals formed (4 mg, yield: 57%).

^{1}H-NMR (500 MHz, DMSO-d_6) δ 8.24 (d, *J* = 7.8 Hz, 1H), 7.90 (t, *J* = 7.6 Hz, 1H), 7.83 (t, *J* = 7.6 Hz, 1H), 7.75 (t, *J* = 6.0 Hz, 2H), 7.47 (d, *J* = 7.6 Hz, 1H), 6.94 (s, 2H), 6.80 (s, 2H), 3.94 (q, *J* = 7.0 Hz, 2H), 3.49 (p, *J* = 7.2 Hz, 4H), 2.10 (s, 6H), 1.26 (t, *J* = 7.2 Hz, 6H), 0.84 (t, *J* = 7.1 Hz, 3H).

All the crystals powder were collected by filtration, washed with diethyl ether and dried in vacuum.

2. Raman Spectra

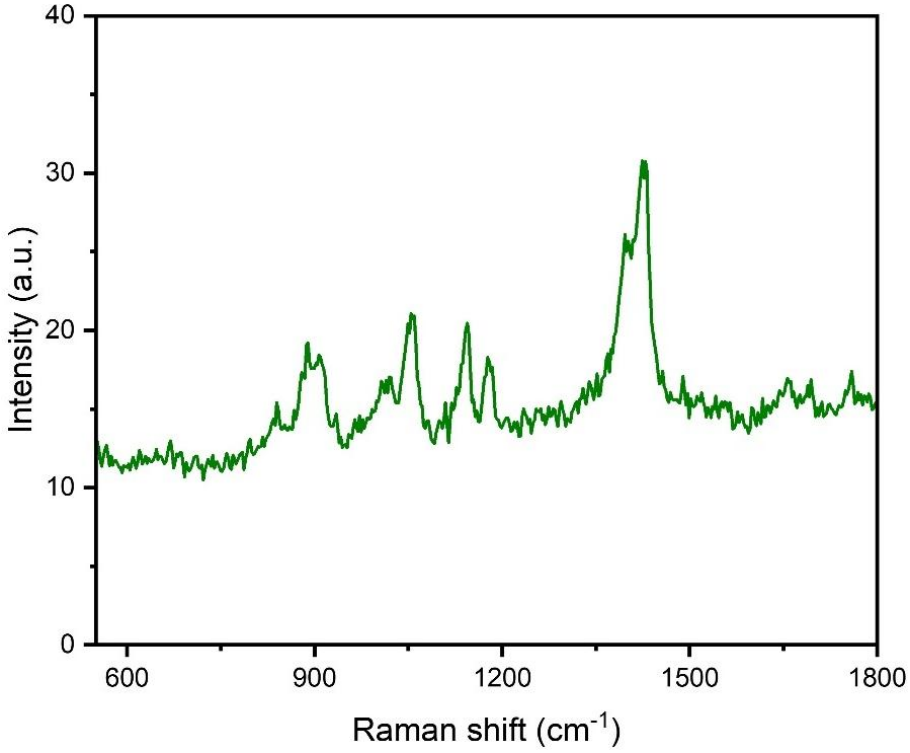

Figure S1. Raman spectrum of the [**Ni**] single crystal (λ_{ex} = 532 nm).

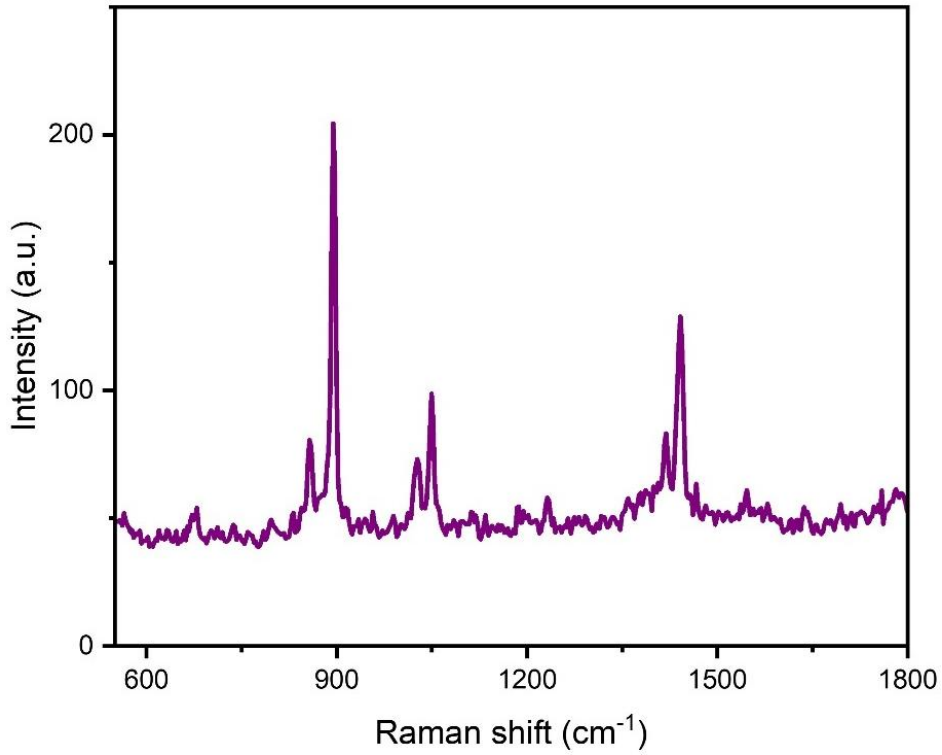

Figure S2. Raman spectrum of the [**Pd**] single crystal (λ_{ex} = 532 nm).

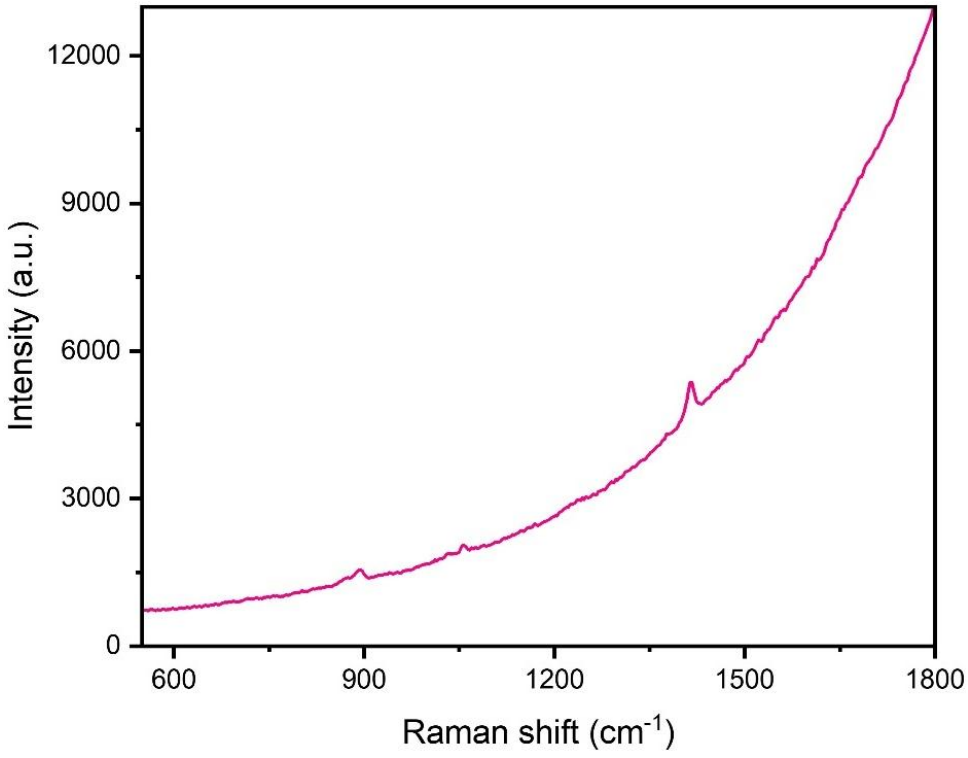

Figure S3. Raman spectrum of the [**Zn**] single crystal (λ_{ex} = 532 nm).

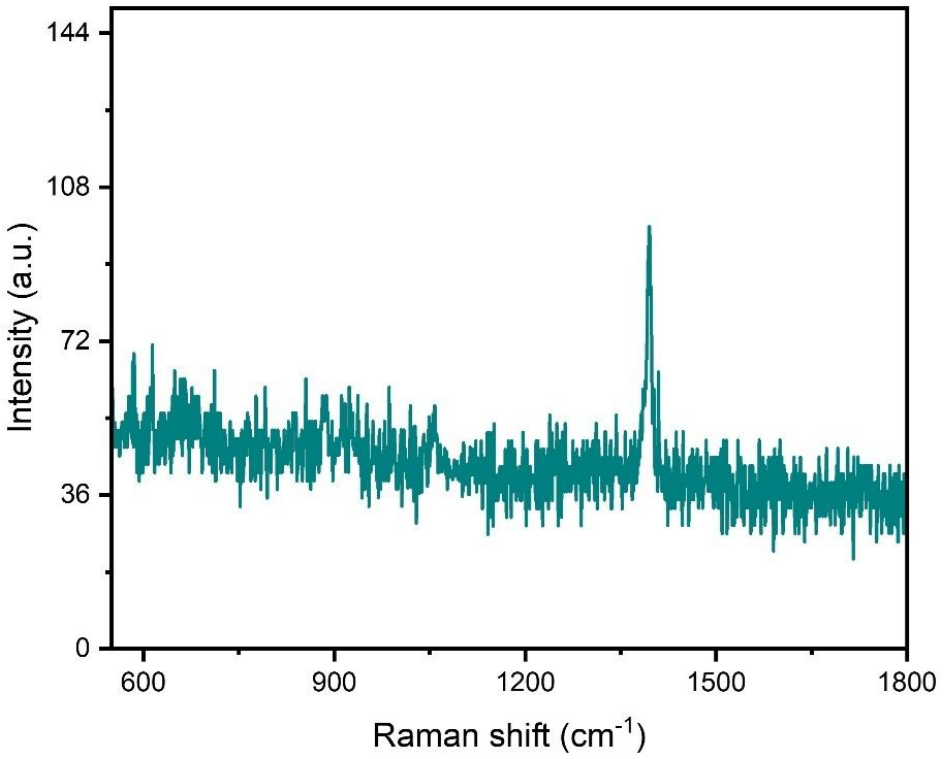

Figure S4. Raman spectrum of **Ni-2** single crystal with 785 nm excitation wavelength.

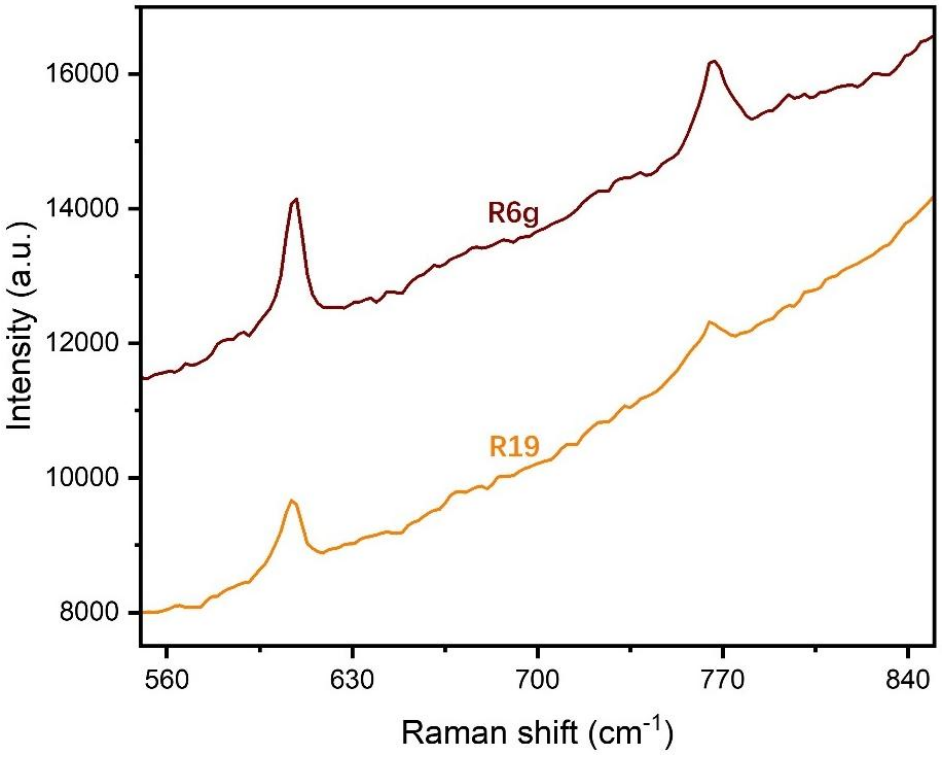

Figure S5. Averaged Raman spectrum of **R6G** and **R19** dried from their respective solution with concentration = 1×10^{-3} M.

*Raw data of **R19/R6G+M** at specific concentrations*

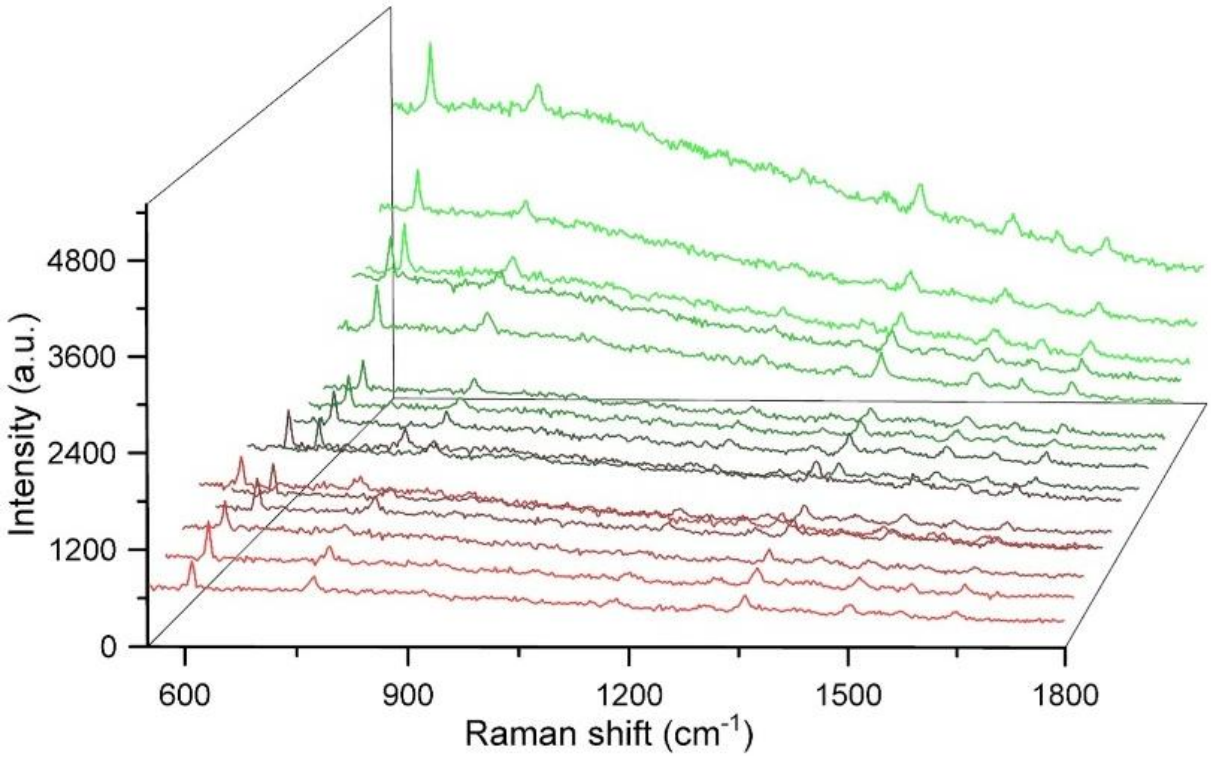

Figure S6. Raman spectra of mixed solution dried on the Si substrate: [**R19**] = 1×10^{-6} M & [**Ni**] = 5×10^{-5} M (λ_{ex} = 532 nm).

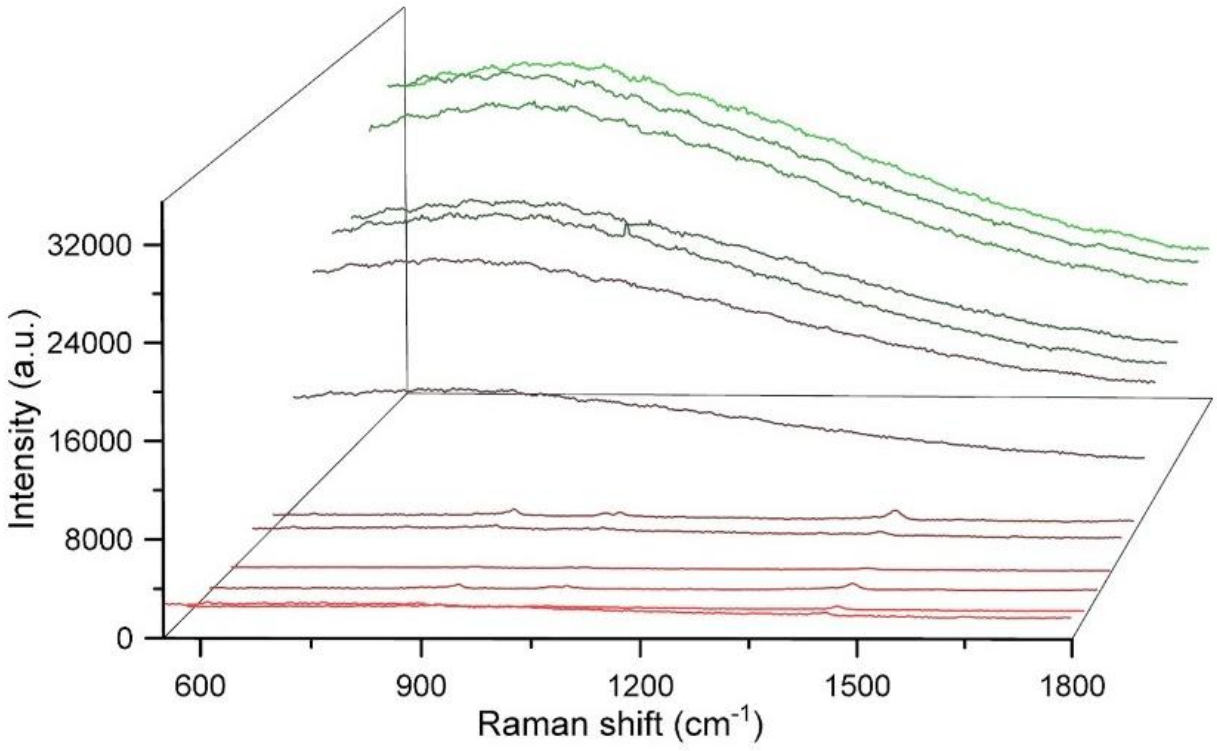

Figure S7. Raman spectra of mixed solution dried on the Si substrate: [**R19**] = 1×10^{-6} M & [**Pd**] = 5×10^{-5} M (λ_{ex} = 532

nm).

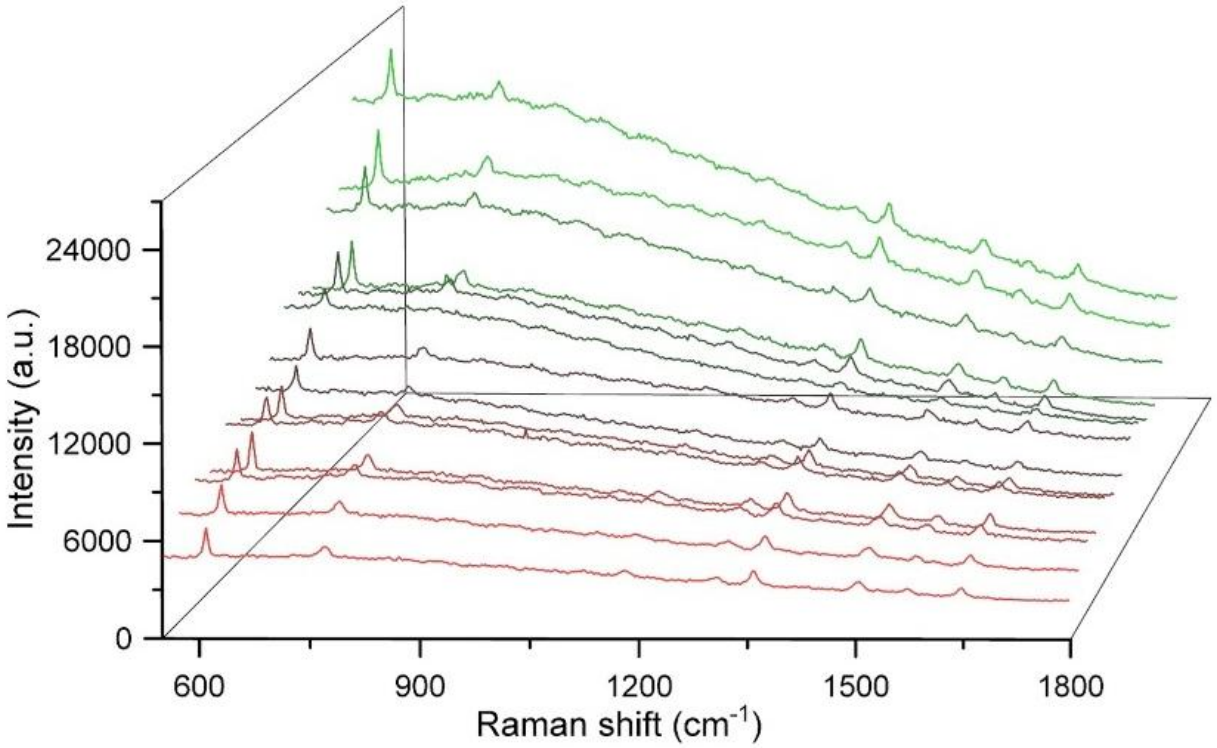

Figure S8. Raman spectra of mixed solution dried on the Si substrate: [**R19**] = 1×10^{-6} M & [**Ni**] = 1×10^{-5} M (λ_{ex} = 532 nm).

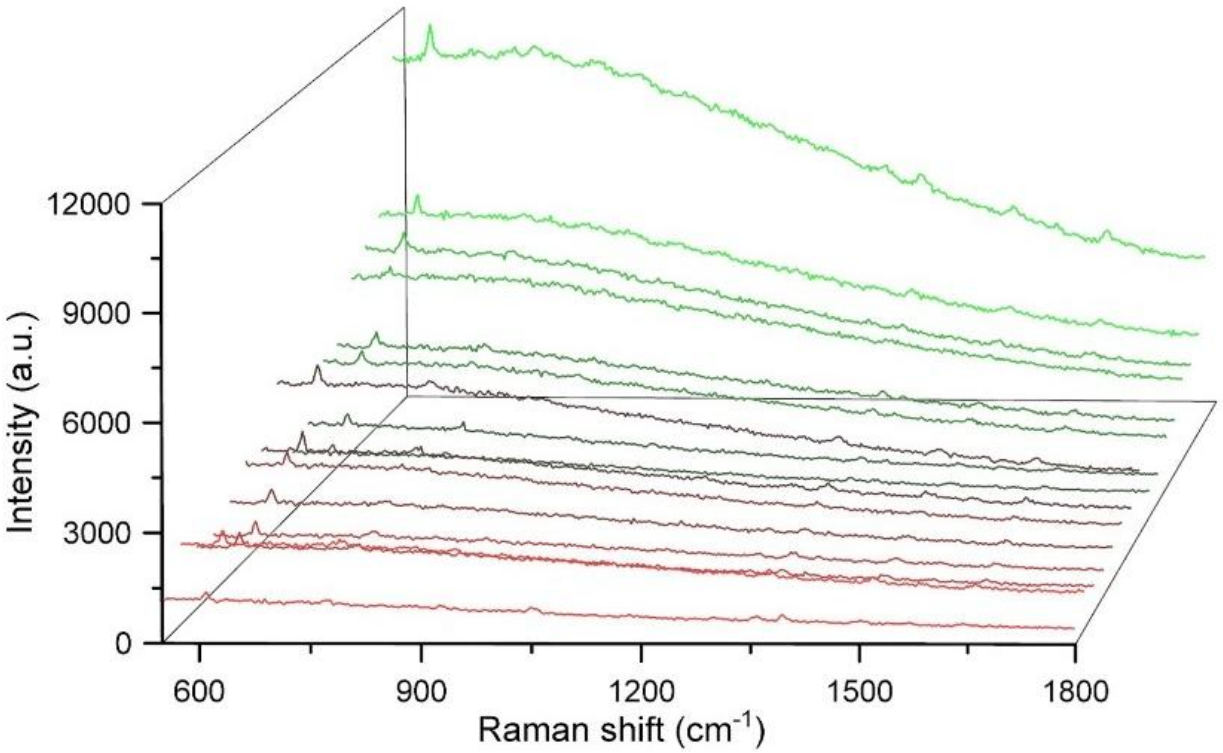

Figure S9. Raman spectra of mixed solution dried on the Si substrate: [**R19**] = 1×10^{-6} M & [**Ni**] = 1×10^{-4} M (λ_{ex} = 532 nm).

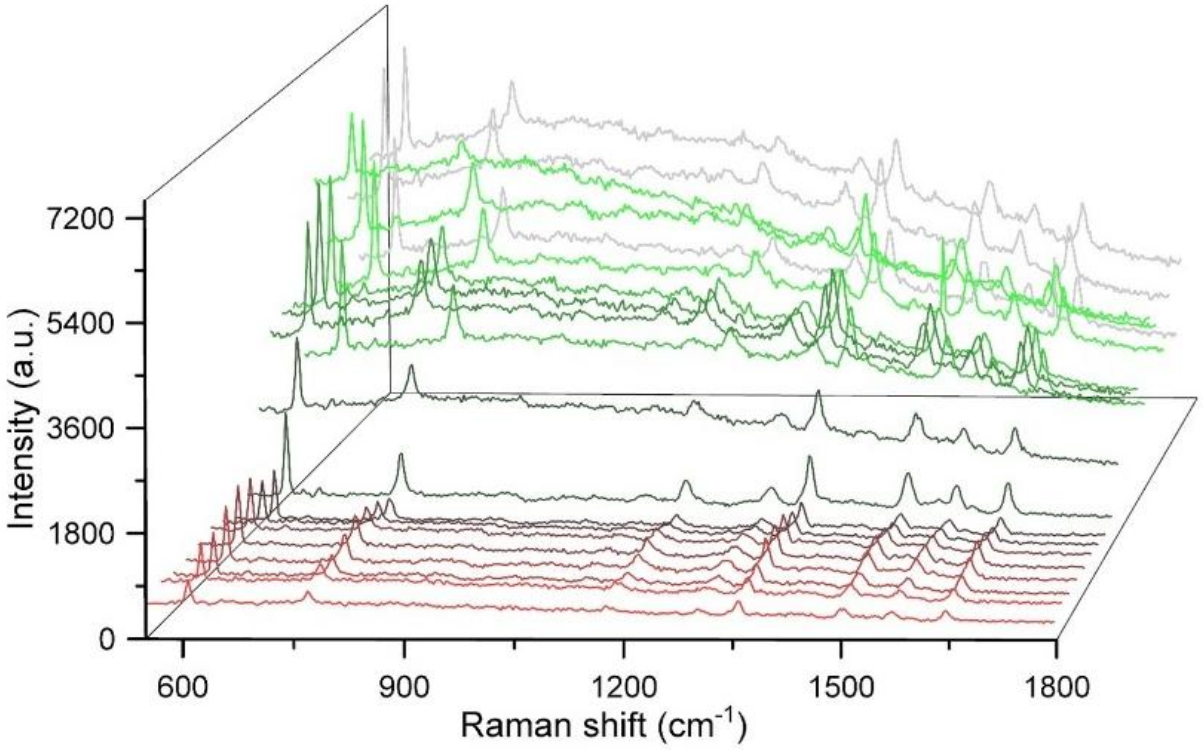

Figure S10. Raman spectra of mixed solution dried on the Si substrate: [**R6G**] = 1×10^{-6} M & [**Ni**] = 5×10^{-5} M (λ_{ex} = 532 nm).

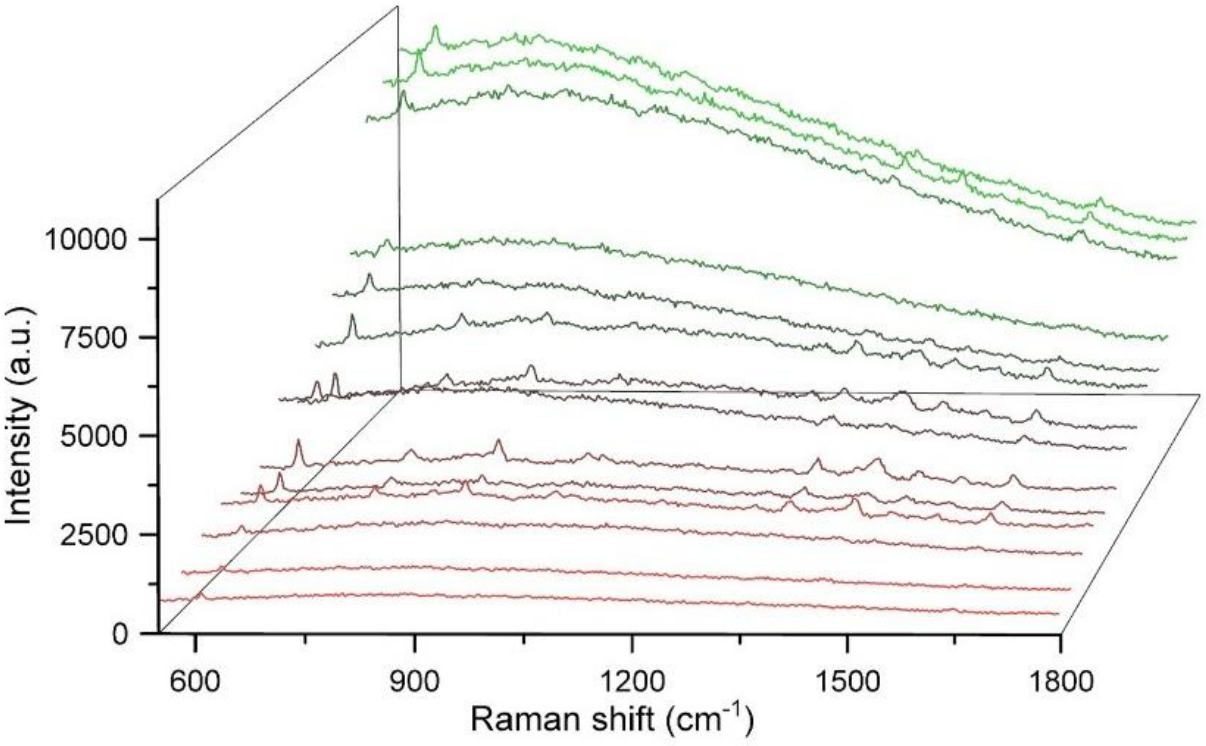

Figure S11. Raman spectra of mixed solution dried on the Si substrate: [**R6G**] = 1×10^{-6} M & [**Pd**] = 5×10^{-5} M (λ_{ex} = 532

nm).

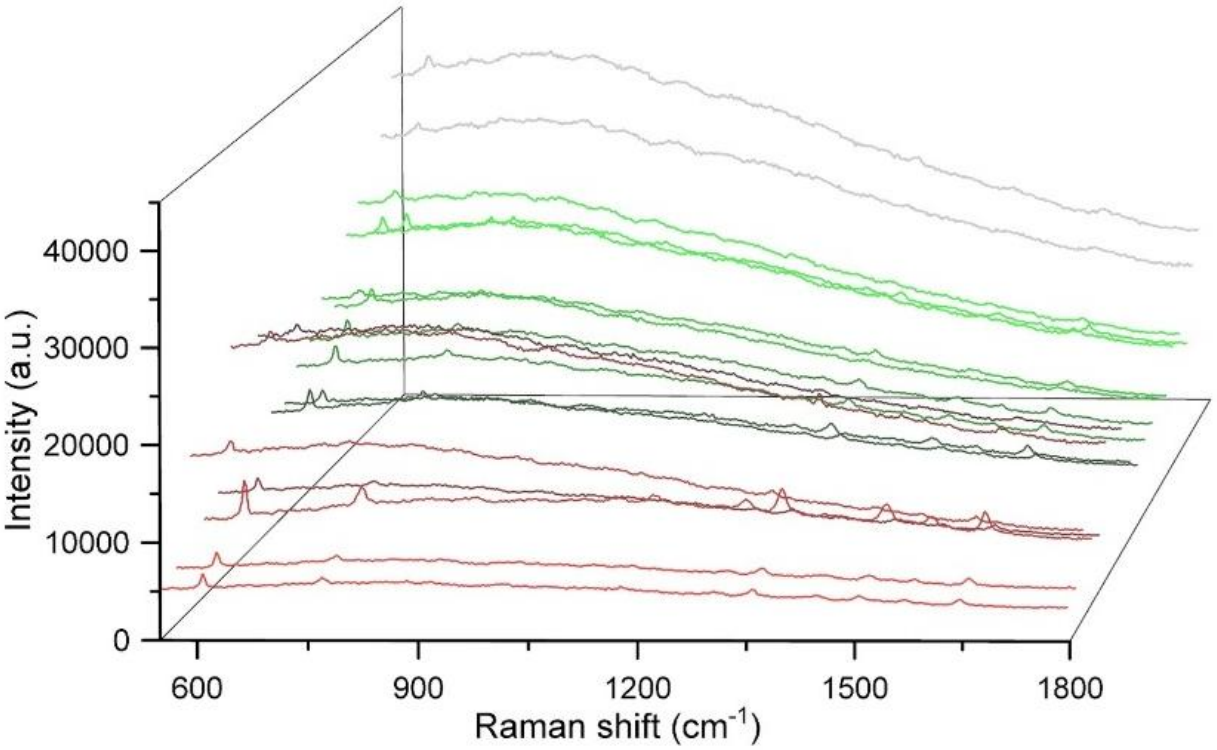

Figure S12. Raman spectra of mixed solution dried on the Si substrate: [**R6G**] = 1×10^{-6} M & [**Ni**] = 1×10^{-5} M (λ_{ex} = 532 nm).

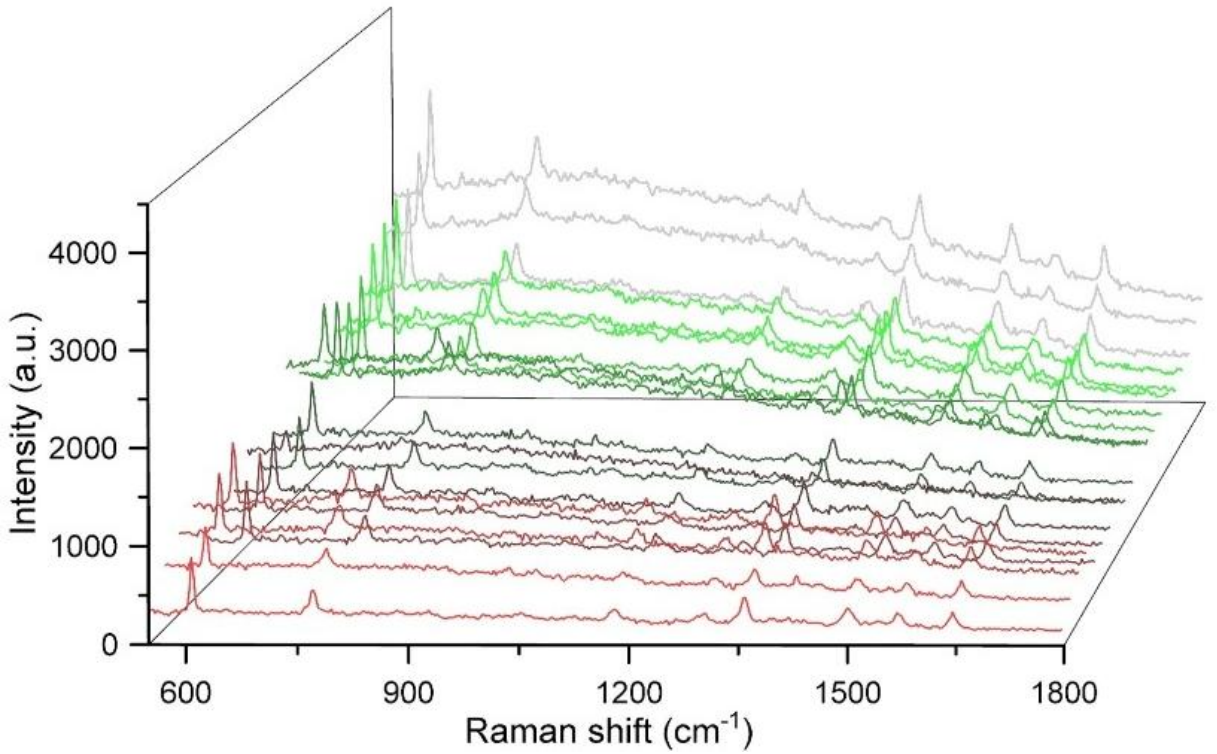

Figure S13. Raman spectra of mixed solution dried on the Si substrate: [**R6G**] = 1×10^{-6} M & [**Ni**] = 1×10^{-4} M (λ_{ex} = 532 nm).

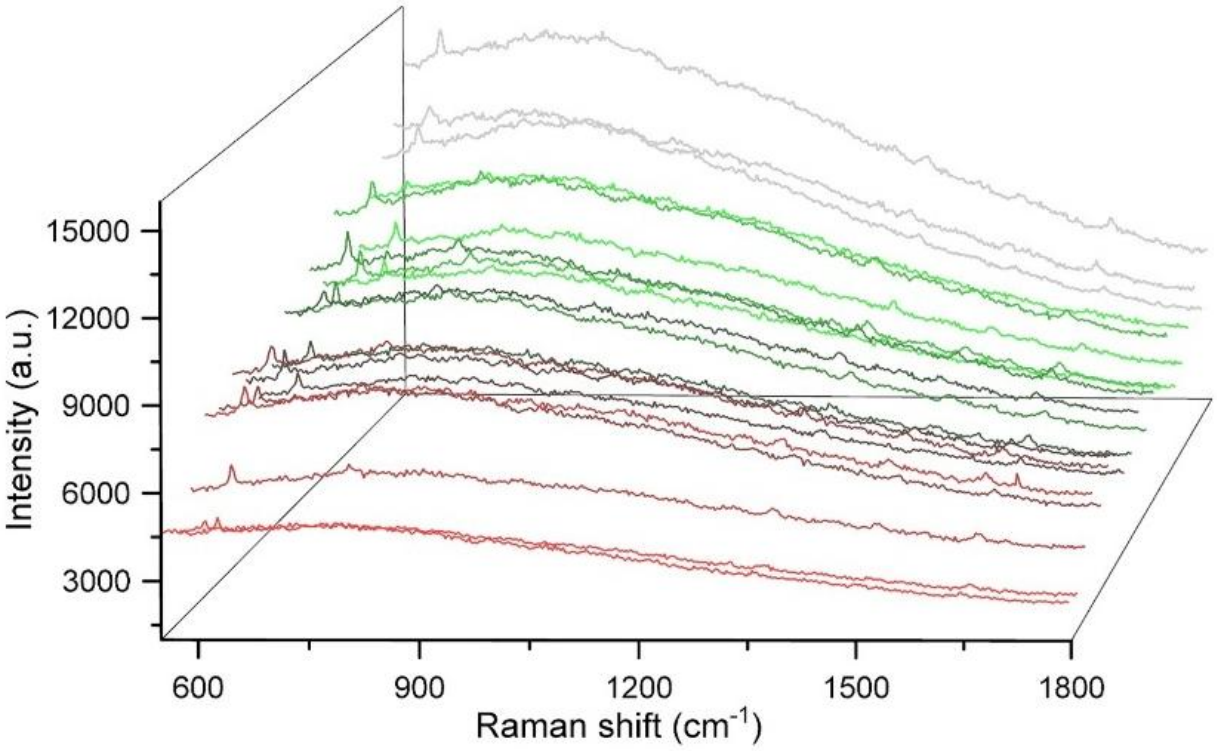

Figure S14. Raman spectra of mixed solution dried on the Si substrate: [**R6G**] = 1×10^{-7} M & [**Ni**] = 1×10^{-5} M (λ_{ex} = 532 nm).

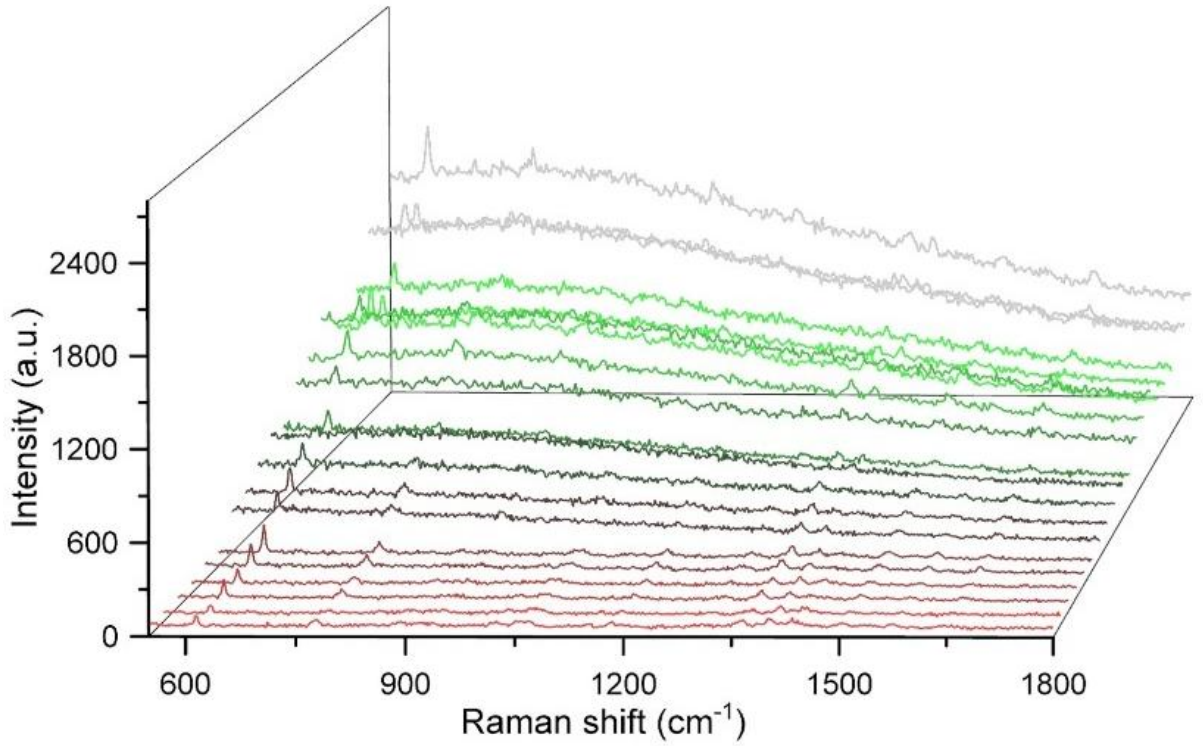

Figure S15. Raman spectra of mixed solution dried on the Si substrate: [**R6G**] = 1×10^{-8} M & [**Ni**] = 1×10^{-5} M (λ_{ex} = 532 nm).

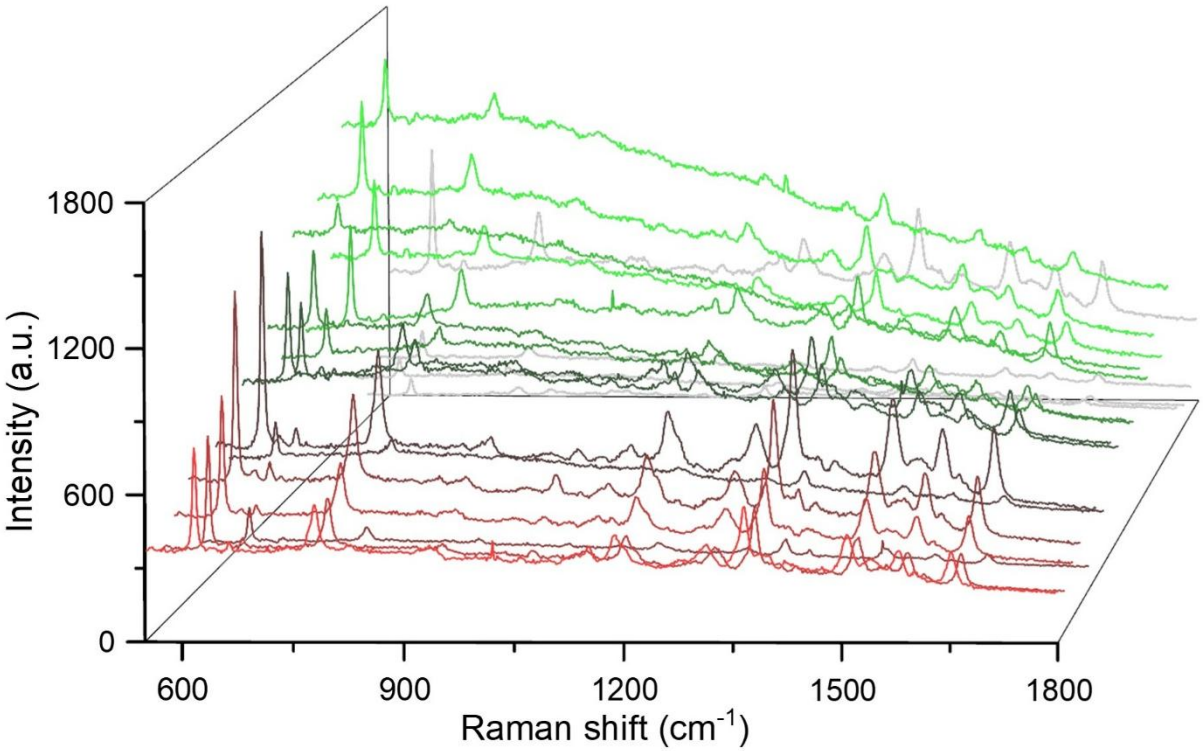

Figure S16. Raman spectrum in the PBS buffer dried on the Si substrate: 10^{-6} M **R6G** molecule with 5×10^{-5} M [**Ni**] dried

from the solution of PBS : ACN (95% : 5%, volume/volume). All Raman spectra were recorded under excitation at 532 nm.

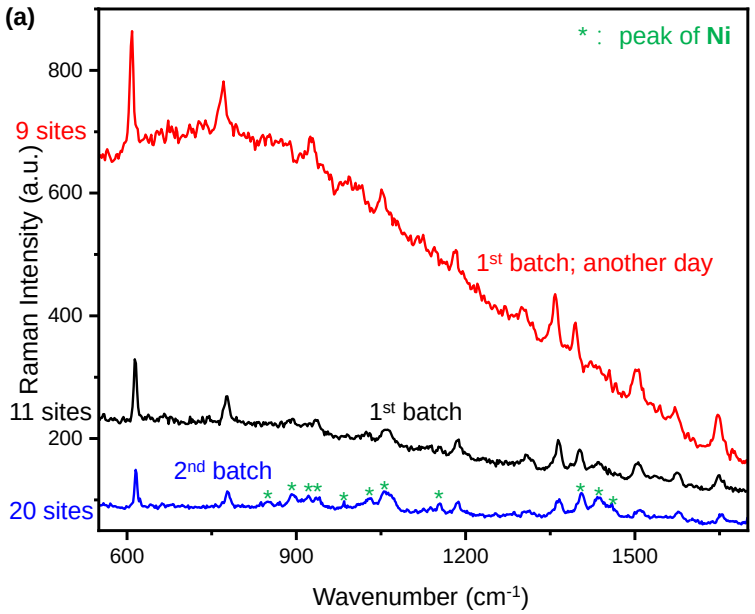

(b)

	S	N	SNR
1st batch; another day	189	38.9	4.86
1st batch	102.3	18.7	5.47
2nd batch	64.9	13.3	4.88

Figure S17. (a) Averaged Raman spectra of mixed solution dried on the Si substrate: [**R6G**] = 1×10^{-8} M & [**Ni**] = 1×10^{-5} M (λ_{ex} = 532 nm), measured from different batches and on different days. (b) Corresponding signal-to-noise ratio (SNR) value of the data shown in (a) at 608 cm^{-1}.

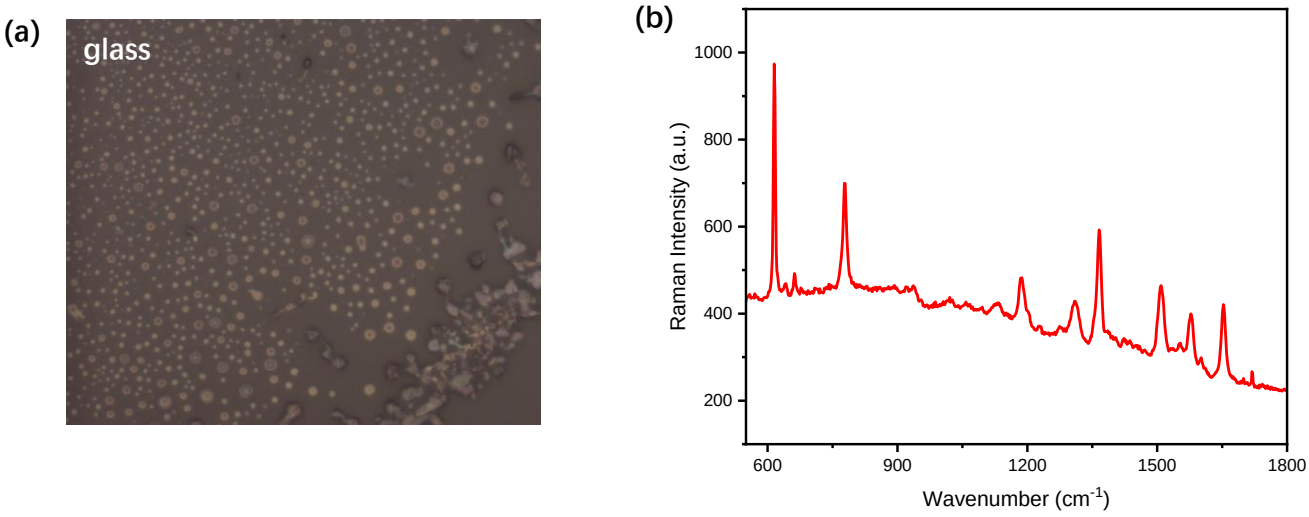

Figure S18. (a) Optical images of a glass substrate after drying from a mixed solution containing [**R6G**] = 1 × 10^{-6} M and [**Ni**] = 5 × 10^{-5} M. (b) Average Raman spectrum acquired from 20 sites on the glass substrate (λ_{ex} = 532 nm).

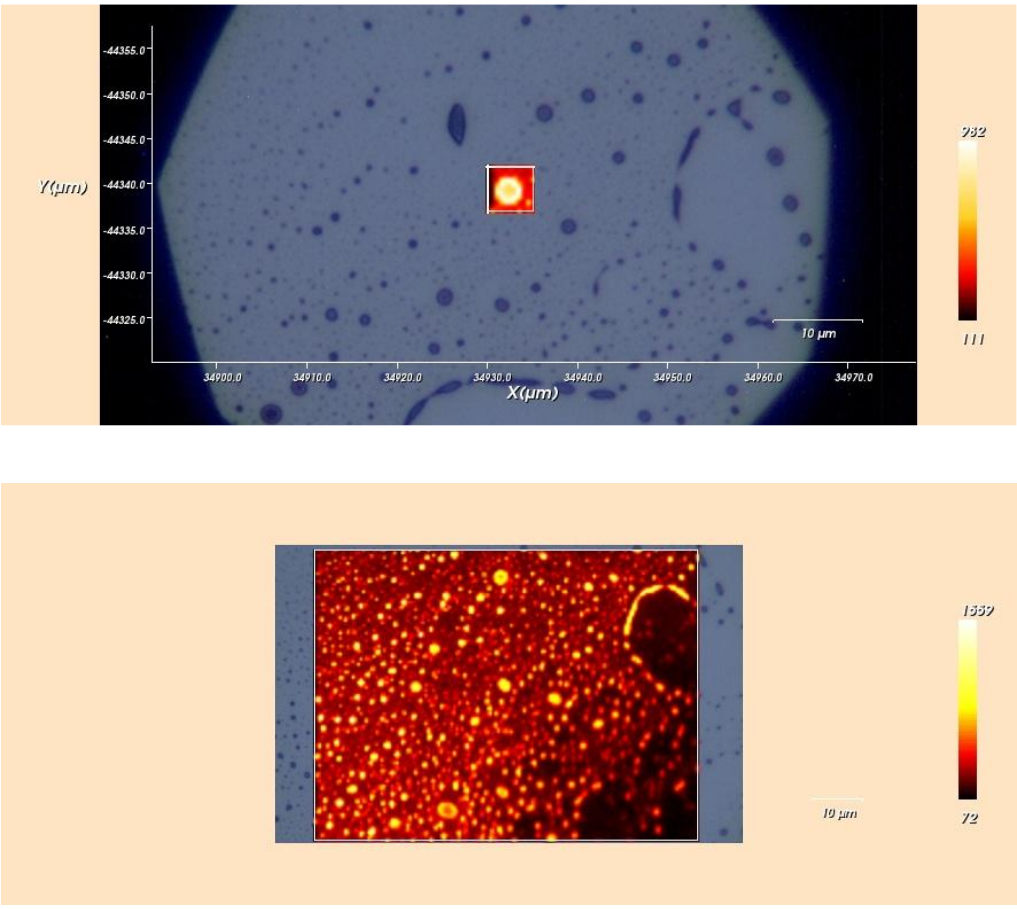

Figure S19. Raman mapping image at 608 cm^{-1} of the sample prepared from a solution containing 1 × 10^{-6} M **R6G** and 1 × 10^{-5} M [**Ni**] in acetonitrile, dried on a Si substrate. (λ_{ex} = 532 nm)

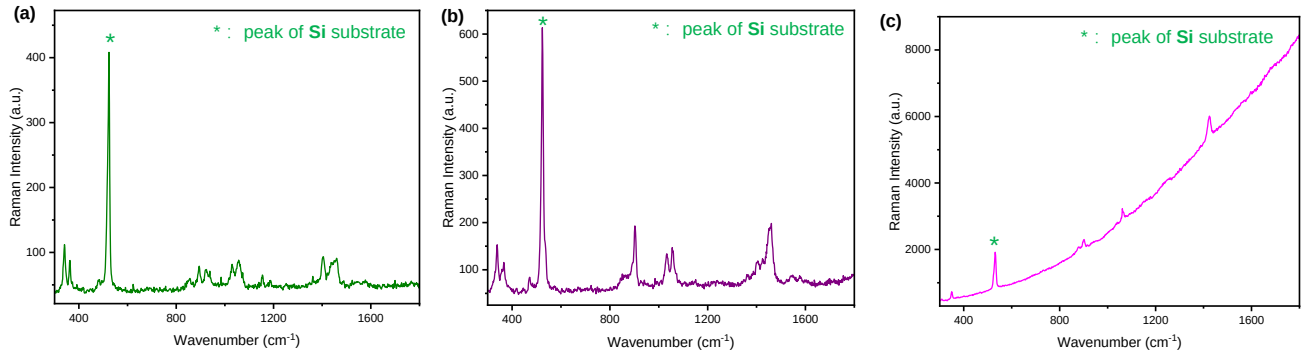

Figure S20. Raman spectra of (a) [**Ni**], (b) [**Pd**], and (c) [**Zn**] after drying from 5 × 10^{-5} M acetonitrile solutions on a Si substrate. (λ_{ex} = 532 nm)

3. EF (Enhanced Factor)

The EF was calculated according to the following formula.[1,2]

$$EF = \frac{(\frac{I}{N})}{(\frac{I_{reference}}{N_{reference}})} \quad (1)$$

$$N \text{ or } N_{reference} = CVN_A \frac{A_{Raman}}{A_{sub}} \quad (2)$$

$$SD = \sqrt{\frac{\sum_{i=1}^{n}(x_i - \bar{x})^2}{n-1}} \quad (3)$$

$$95\%CI = 1.96 \times \frac{SD}{\sqrt{n}} \quad (4)$$

Here, I and $I_{reference}$ represent enhanced and normal Raman intensities, while N and $N_{reference}$ denote the number of **R19**/**R6G** molecules contributing to these signals. For analyte molecules on Si/SiO_2 wafers, N and $N_{reference}$ were estimated assuming uniform distribution, where C is molar concentration (molecular platform developed in this work: 1×10^{-6} M **R19**/**R6G** + 5×10^{-5} M **Ni**/**Pd**; reference: 1×10^{-3} M **R19**/**R6G**), V is droplet volume (5 μL), N_A is Avogadro's constant, A_{Raman} is laser spot area (44.2 μm^2), and A_{sub} is effective substrate area. SD and 95%CI represent sample standard deviation and 95% confidence interval (normal distribution). n is the sample size and $\bar{x}$ represents the mean.

Table S1. EF of **R19**/**R6G**, accounting for CT effects.

Probe Molecule	CT complex	Mean of EF	SD	95%CI
R19	**Ni**	475.1	111.2	54.5
R19	**Pd**	130.5	54.3	29.5
R6g	**Ni**	860.8	346.8	152.0
R6g	**Pd**	336.8	78.7	41.2

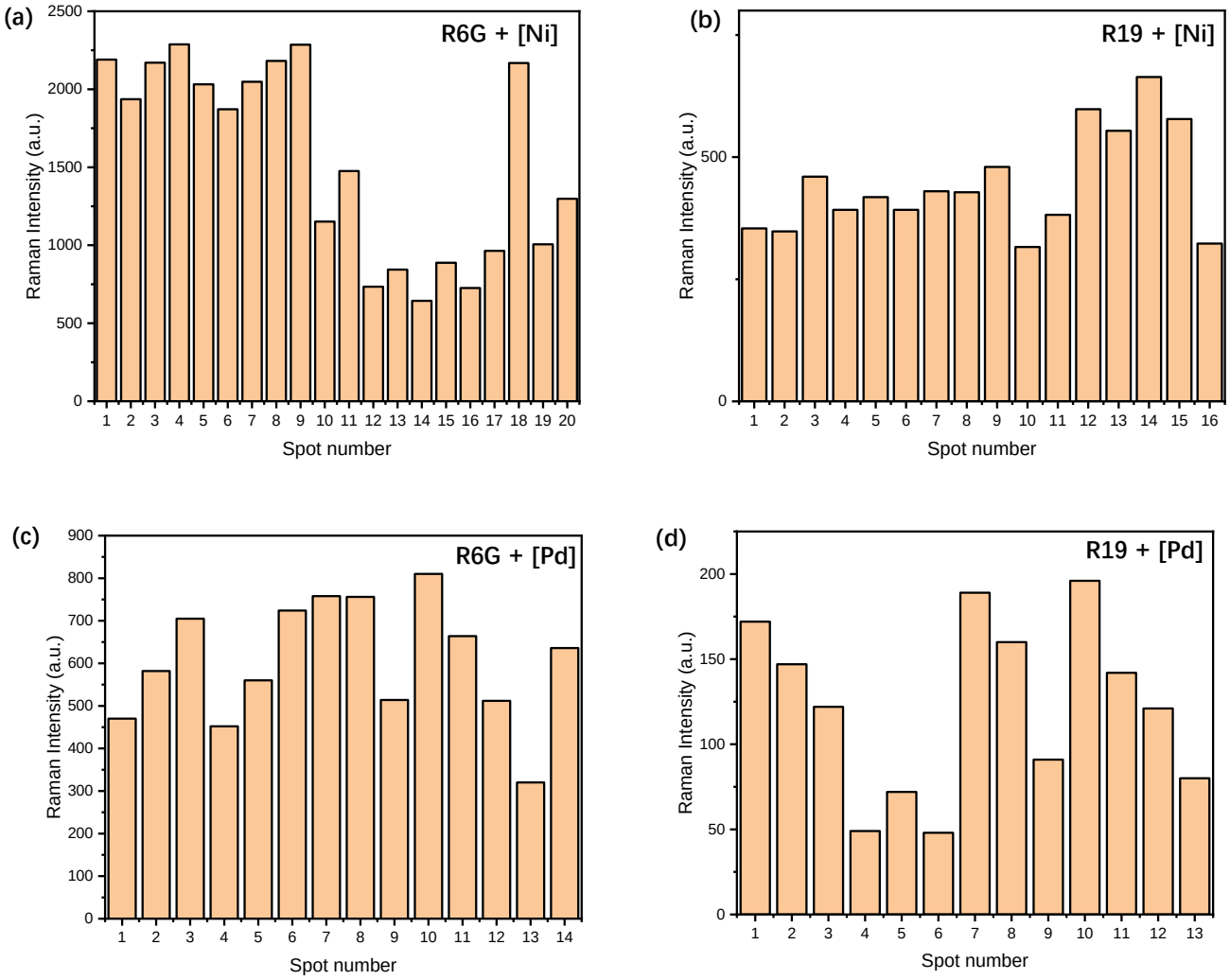

Figure S21. Distribution plots of the Raman intensity for samples of (a) [**R6G**] + [**Ni**], (b) [**R19**] + [**Ni**], (c) [**R6G**] + [**Pd**], (d) [**R19**] + [**Pd**], under the condition of [**R19/R6G**] = 1×10^{-6} M & [**Ni/Pd**] = 5×10^{-5} M in acetonitrile, dried on a Si substrate. (λ_{ex} = 532 nm) The Raman intensities were extracted at 608 cm^{-1} based on the spectra shown in Figure S6-S7 and S10-S11.

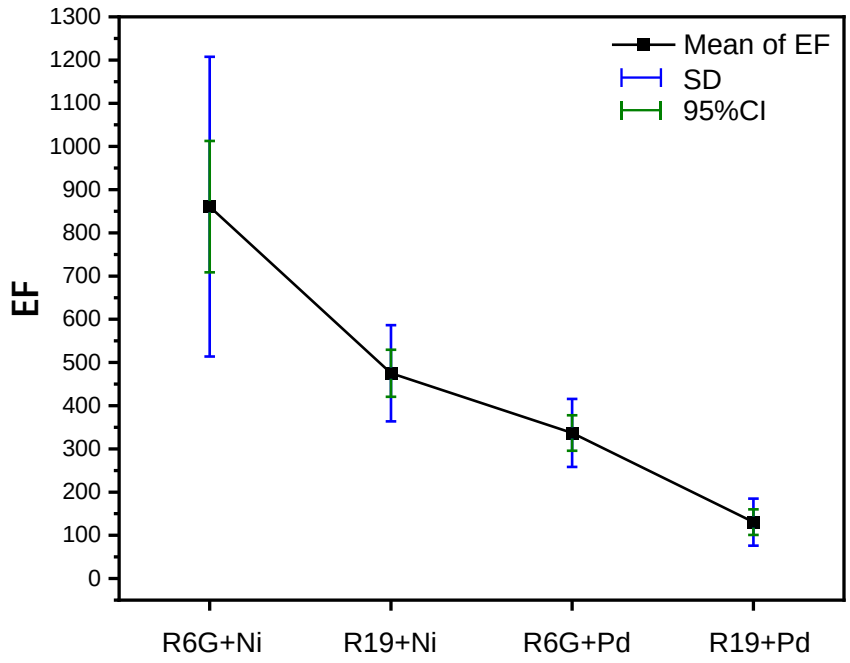

Figure S22. Enhancement factor (EF) values presented as mean ± standard deviation (SD) with 95% confidence intervals (CI), calculated from the distribution plots in Figure S21.

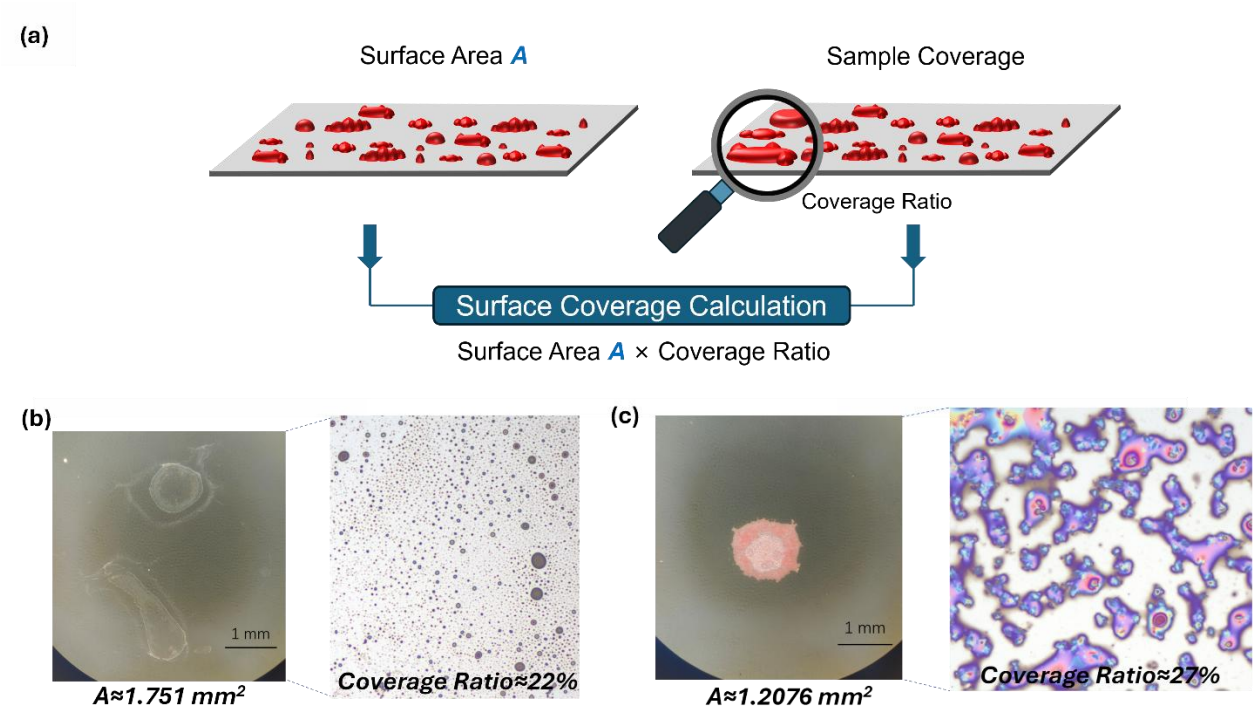

Figure S23. (a) An illustration scheme to calculate the surface coverage after drying. (b-c) Optical microscopy images showing surface coverage and coverage ratio of the dried residue from an acetonitrile solution containing (b) [**R6G**] = 1 × 10^{-6} M and [**Ni**] = 1 × 10^{-5} M on a Si substrate, and (c) [**R6G**] = 1 mM on a Si substrate.

4. Reflectance Spectra

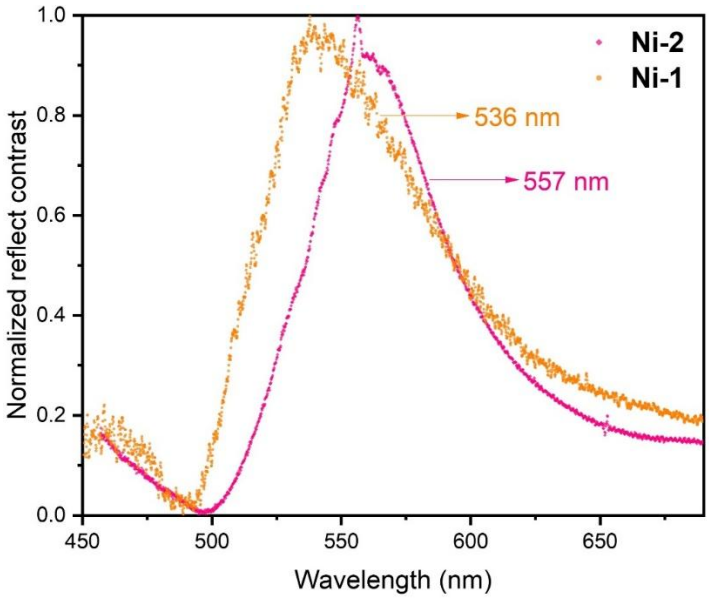

Figure S24. Reflectance spectra of **Ni-1/2** single crystals

5. UV-vis Spectra

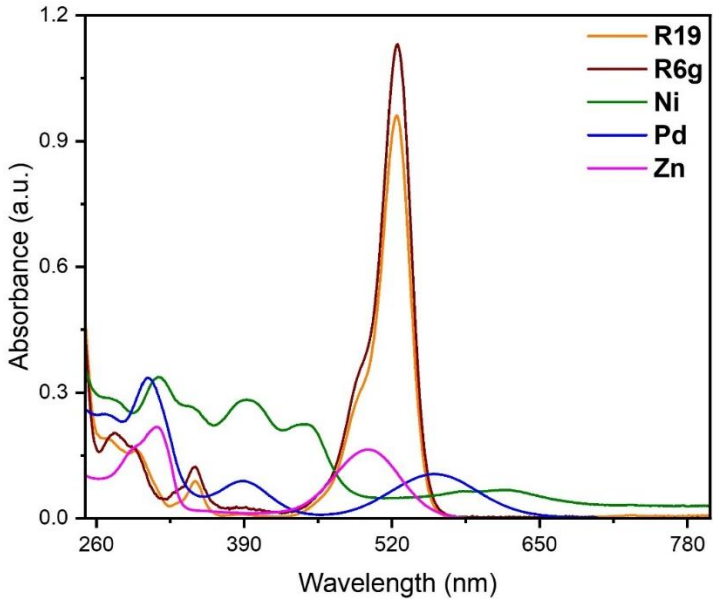

Figure S25. UV-vis spectra in acetonitrile at a concentration of 1×10^{-5} M.

6. ^{1}H-NMR Spectra

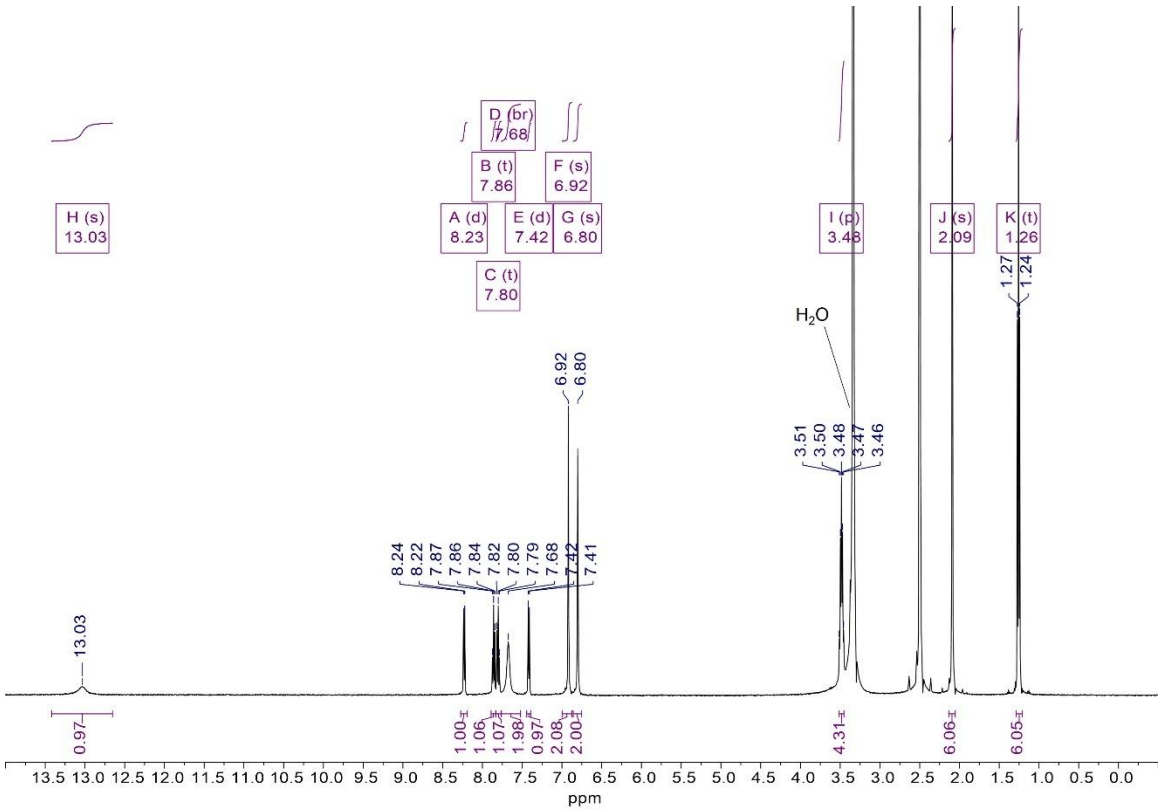

Figure S26. [1]H-NMR spectra of **R19** in DMSO-d_6.

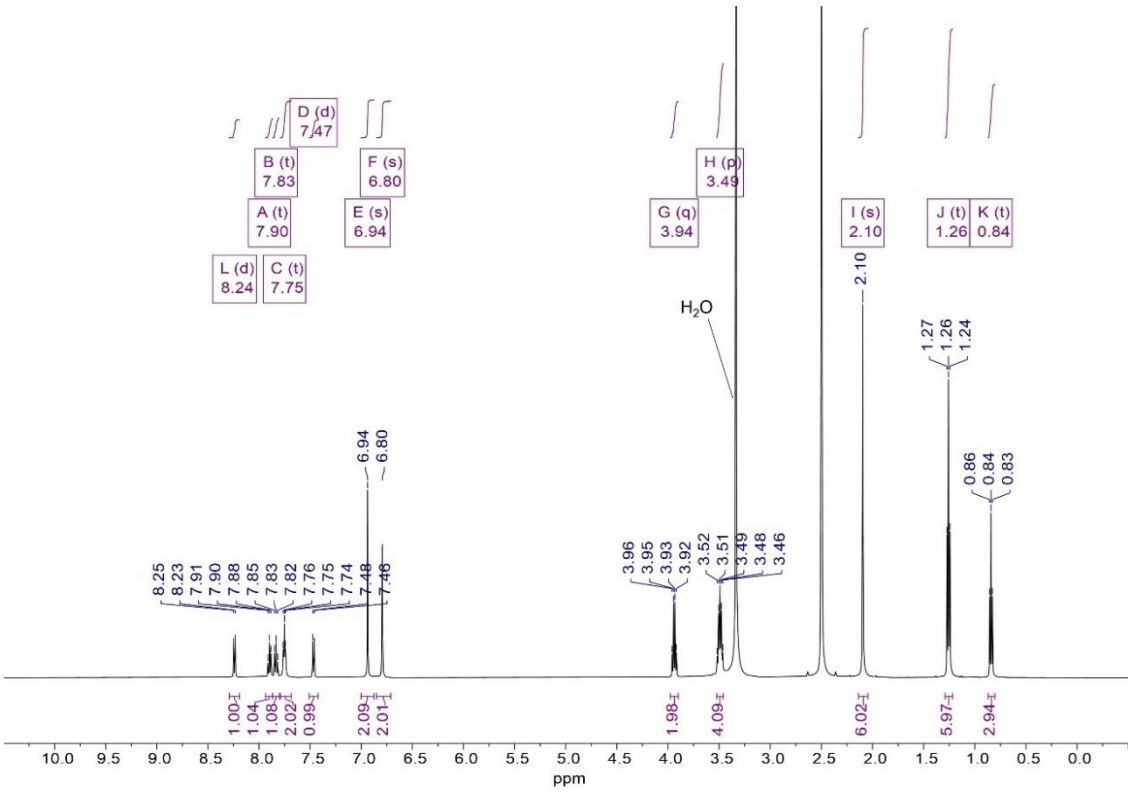

Figure S27. [1]H-NMR spectra of **R6G** in DMSO-d_6.

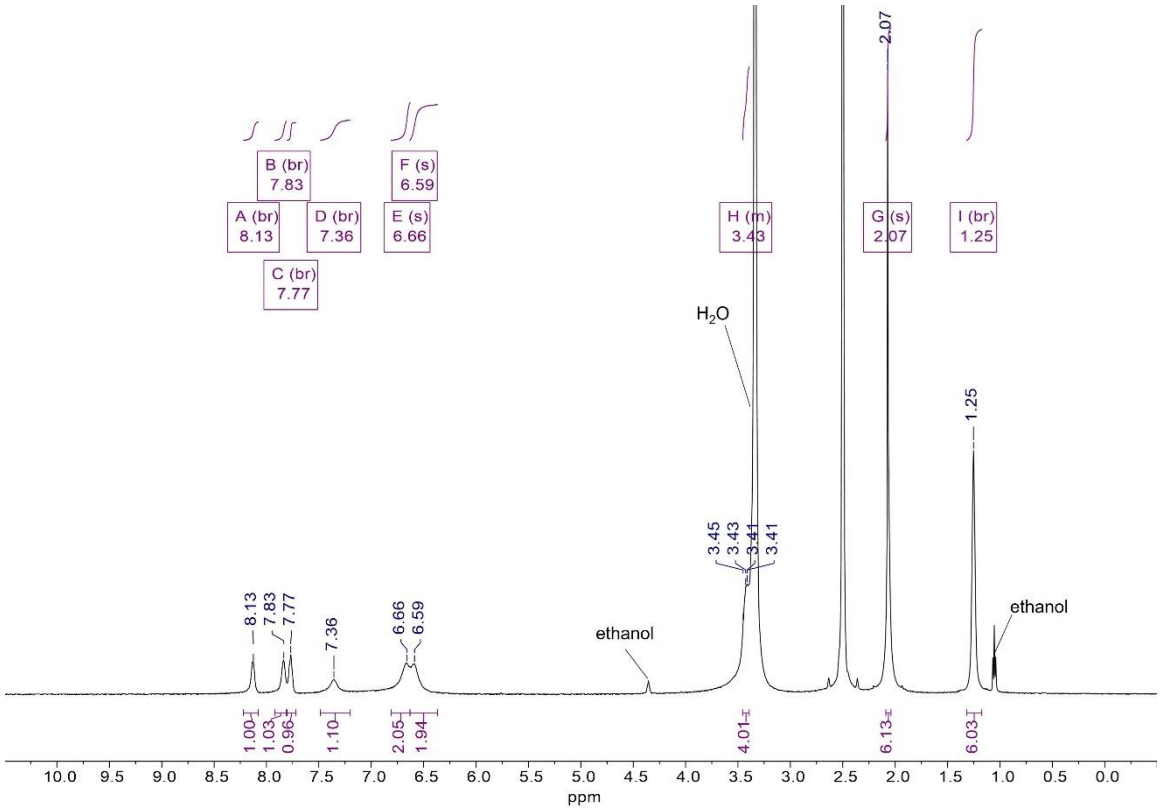

Figure S28. [1]H-NMR spectra of **Ni-1** in DMSO-d_6.

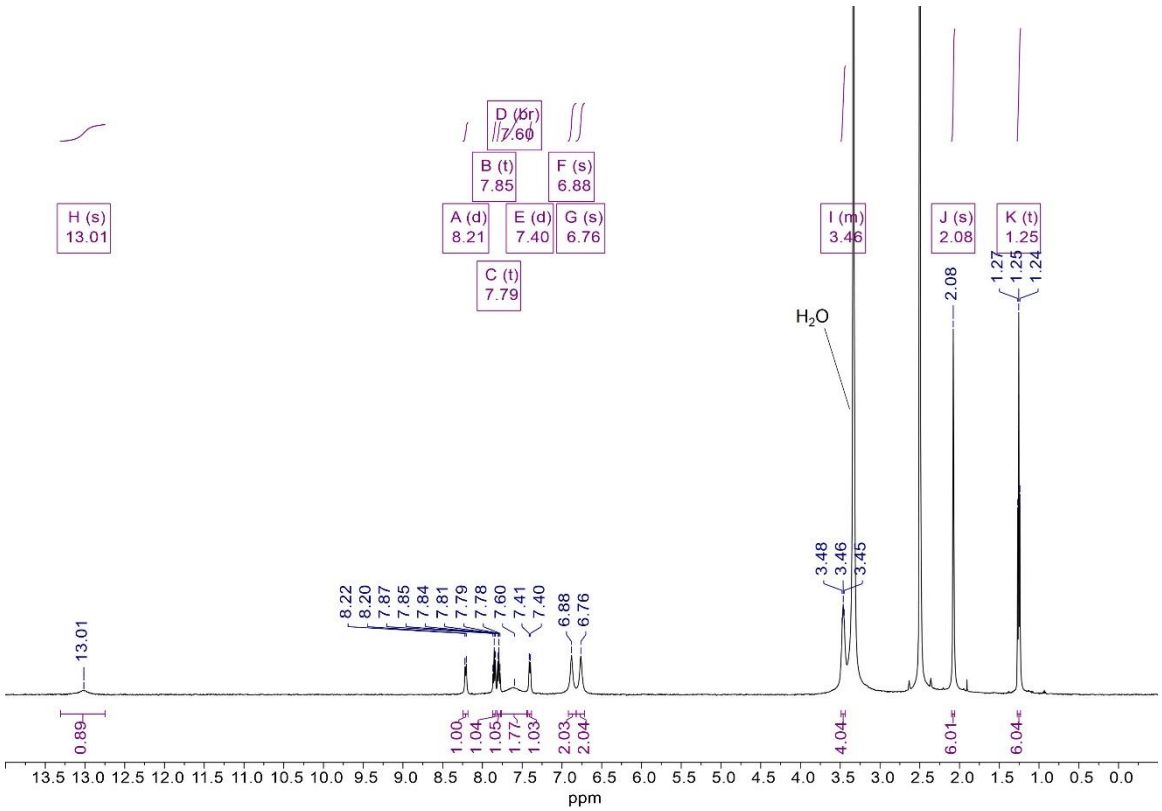

Figure S29. [1]H-NMR spectra of **Pd-1** in DMSO-d_6.

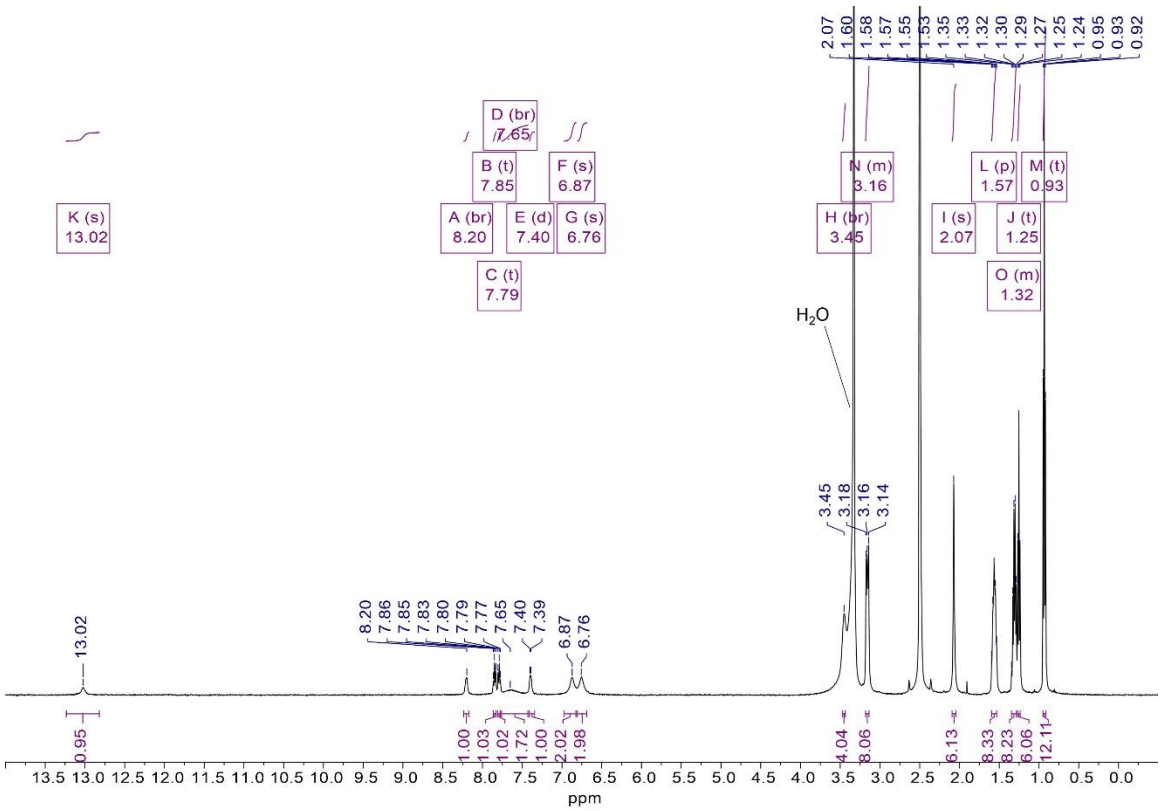

Figure S30. [1]H-NMR spectra of **Zn-1** in DMSO-d_6.

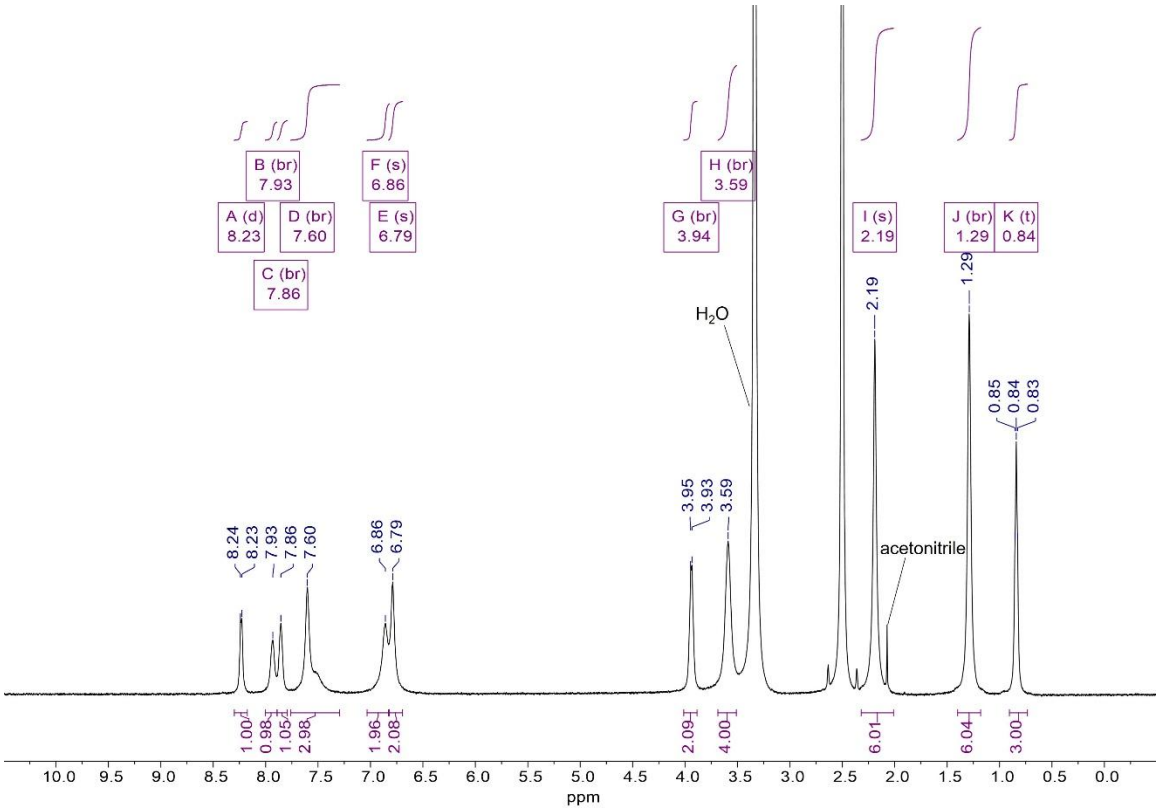

Figure S31. [1]H-NMR spectra of **Ni-2** in DMSO-d_6.

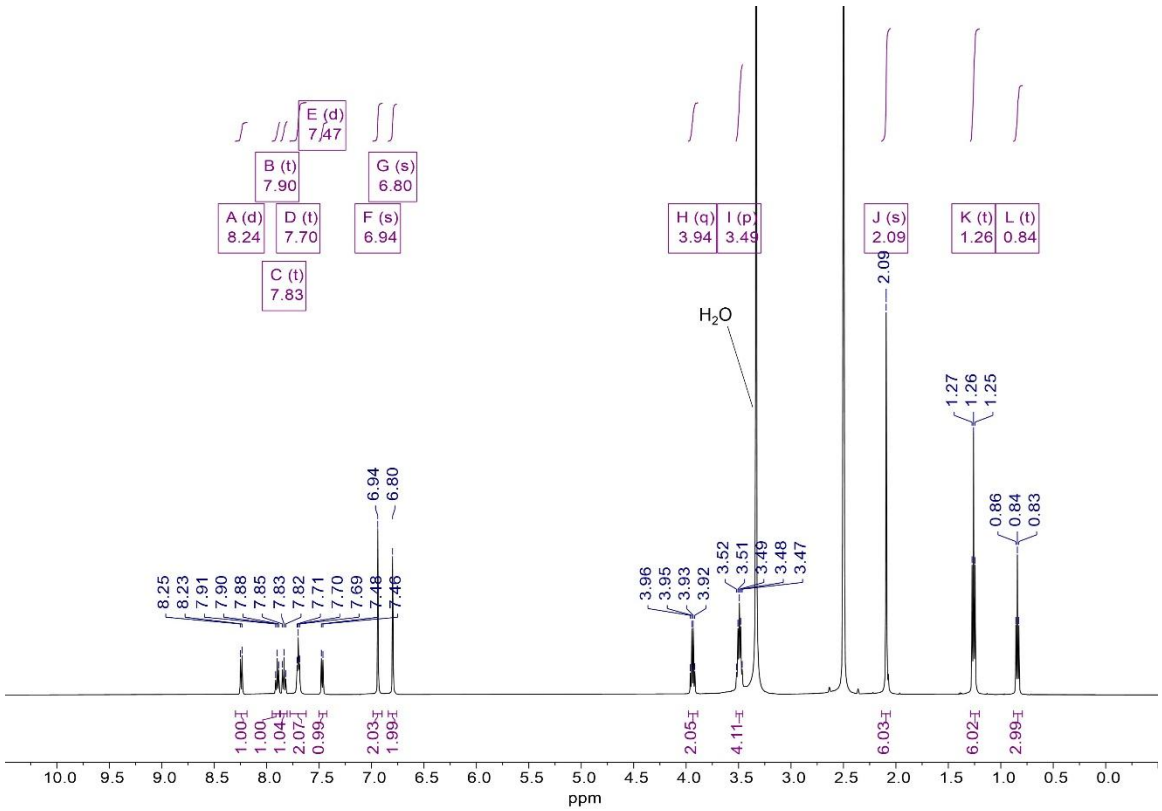

Figure S32. [1]H-NMR spectra of **Pd-2** in DMSO-d_6.

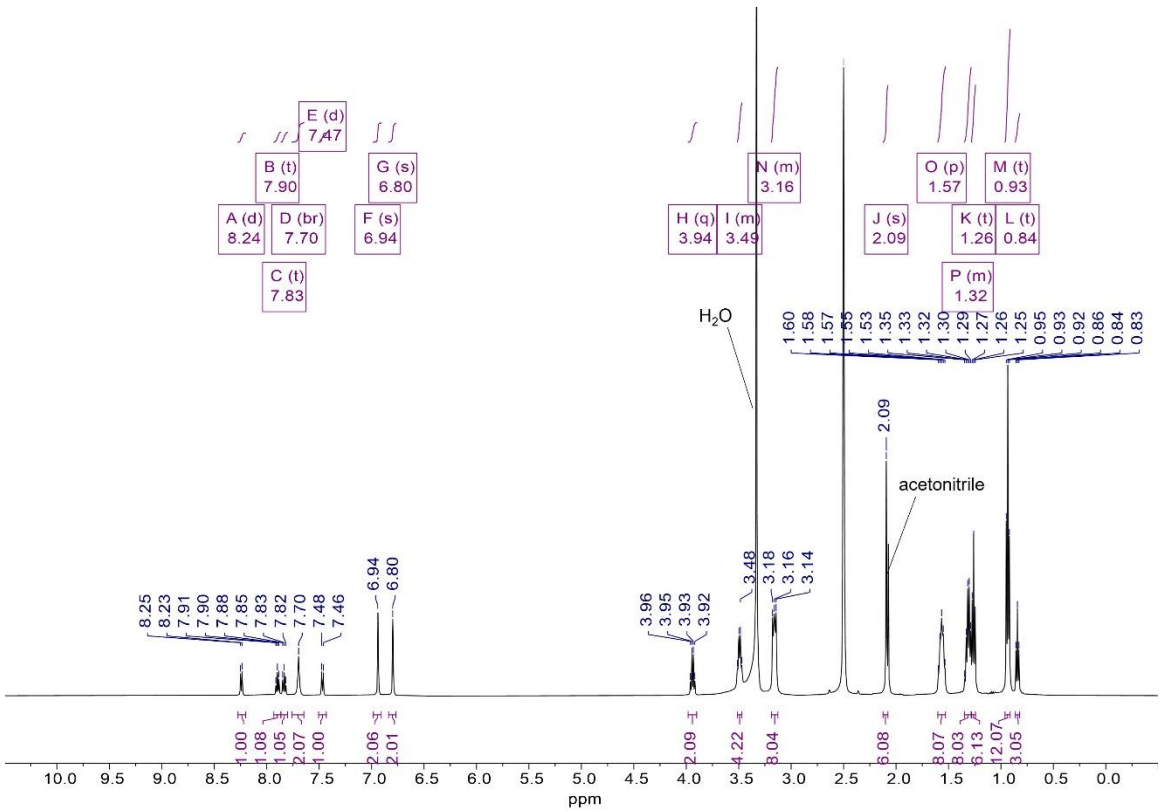

Figure S33. [1]H-NMR spectra of **Zn-2** in DMSO-d_6.

7. Refinement Data of the X-ray Structures

Table S2. Crystal data and structure refinements for **Ni-1** (CCDC: 2479924) and **Ni-2** (CCDC: 2479921).

	Ni-1	**Ni-2**
Empirical formula	$C_{34}H_{33}N_2NiO_4S_{10}$	$C_{34}H_{31}N_2NiO_3S_{10}$
Formula weight	912.93	894.92
Temperature / K	296(2)	293(2)
Crystal system	Triclinic	Monoclinic
Space group	P-SS1	$P2_1/c$
a / Å	11.480(5)	28.6433(12)
b / Å	13.227(5)	11.3115(5)
c / Å	14.218(5)	15.862(3)
α / °	101.118(12)	90
β / °	97.148(13)	105.4380(10)
γ / °	98.529(14)	90
Volume / $Å^3$	2068.8(13)	7856.6(6)
Z	2	8
ρ_{calc} Mg/m^3	1.466	1.513
μ/mm^{-1}	1.012	1.063
F(000)	942	3688
Crystal size / mm^3	0.3x0.2x0.2	0.4×0.3×0.2
Radiation	MoKα (λ = 0.71073)	MoKα (λ = 0.71073)

2θ range for data collection/°	2.396 to 25.250	2.196 to 27.935
Index ranges	−13≤h≤13, −15≤k≤15, −17≤l≤17	−37≤h≤37, −14≤k≤14, −33≤l≤30
Reflections collected	58888	113379
Independent reflections	7491 [R_{int} = 0.0590]	18803 [R(int) = 0.1122]
Data/restraints/parameters	7491/1/469	118803/0/911
Goodness-of-fit on F^2	1.040	1.046
Final R indexes [R>=2σ(I)]	R1 = 0.0434, wR2 = 0.1096	R1 = 0.0843, wR2 = 0.1471
Final R indexes [all data]	R1 = 0.0575, wR2 = 0.1179	R1 = 0.1565, wR2 = 0.1738
Largest diff. peak/hole / $eÅ^{-3}$	0.600/−0.397	1.583 / −0.930

Table S3. Crystal data and structure refinements for **Pd-1** (CCDC: 2479919) and **Pd-2** (CCDC: 2479923).

	Pd-1	**Pd-2**
Empirical formula	$C_{62}H_{60}N_6O_6PdS_{10}$	$C_{62}H_{58}N_4O_6PdS_{10}$
Formula weight	1412.16	1382.12
Temperature / K	304(2)	296(2)
Crystal system	Triclinic	Triclinic
Space group	P-1	P-1
a / Å	8.0052(2)	11.5454(17)
b / Å	12.2415(3)	12.1683(19)
c / Å	17.1514(5)	12.7456(19)
α / °	97.2910(10)	85.850(5)
β / °	103.4270(10)	64.210(5)
γ / °	90.2760(10)	88.366(5)

Volume / $Å^3$	1620.58(7)	1608.0(4)
Z	1	1
ρ_{calc} Mg/m^3	1.447	1.427
μ/mm^{-1}	0.663	0.666
F(000)	728	712
Crystal size / mm^3	0.4x0.3x0.2	0.5×0.4×0.3
Radiation	MoKα (λ = 0.71073)	MoKα (λ = 0.71073)
2θ range for data collection/°	2.463 to 28.018	2.363 to 27.956
Index ranges	−10≤h≤10, −16≤k≤16, −22≤l≤22	−15≤h≤15, −16≤k≤16, −16≤l≤16
Reflections collected	47446	51298
Independent reflections	7793 [R_{int} = 0.0351]	7679 [R(int) = 0.0581]
Data/restraints/parameters	7793/0/417	7679/23/404
Goodness-of-fit on F^2	1.042	1.033
Final R indexes [R>=2σ(I)]	R1 = 0.0327, wR2 = 0.0892	R1 = 0.0440, wR2 = 0.1183
Final R indexes [all data]	R1 = 0.0396, wR2 = 0.0964	R1 = 0.0595, wR2 = 0.1306
Largest diff. peak/hole / $eÅ^{-3}$	0.375/−0.364	0.539 / −0.480

Table S4. Crystal data and structure refinements for **Zn-1** (CCDC: 2479926) and **Zn-2** (CCDC: 2479925).

	Zn-1	**Zn-2**
Empirical formula	$C_{48.25}H_{65}N_3O_{3.50}S_{10}Zn$	$C_{51}H_{69.25}N_3O_3S_{10}Zn$
Formula weight	1129.00	1158.31
Temperature / K	297(2)	296(2)

Crystal system	Triclinic	Triclinic
Space group	P-1	P-1
a / Å	11.5628(16)	13.410(3)
b / Å	13.435(2)	13.585(3)
c / Å	19.579(3)	19.962(4)
α / °	96.172(5)	97.868(7)
β / °	98.566(5)	101.818(7)
γ / °	90.161(5)	118.010(7)
Volume / $Å^3$	2989.7(8)	3026.1(11)
Z	2	2
ρ_{calc} Mg/m^3	1.254	1.271
μ/mm^{-1}	0.799	0.791
F(000)	1187	1220
Crystal size / mm^3	0.4x0.3x0.2	0.5×0.4×0.3
Radiation	MoKα (λ = 0.71073)	MoKα (λ = 0.71073)
2θ range for data collection/°	1.949 to 28.419	2.305 to 27.990
Index ranges	−15≤h≤15, −17≤k≤17, −26≤l≤26	−17≤h≤17, −17≤k≤17, −26≤l≤26
Reflections collected	56093	139592
Independent reflections	14851 [R_{int} = 0.0968]	14536 [R(int) = 0.0482]
Data/restraints/parameters	14851/66/652	14536/27/661
Goodness-of-fit on F^2	1.032	1.091
Final R indexes [R>=2σ(I)]	R1 = 0.0810, wR2 = 0.2269	R1 = 0.0513, wR2 = 0.1498

Final R indexes [all data]	R1 = 0.1649, wR2 = 0.2898	R1 = 0.0631, wR2 = 0.1589
Largest diff. peak/hole / eÅ^{-3}	0.905/−0.621	0.985 / −0.420

8. IV Curves and Conductivities of M-1/2

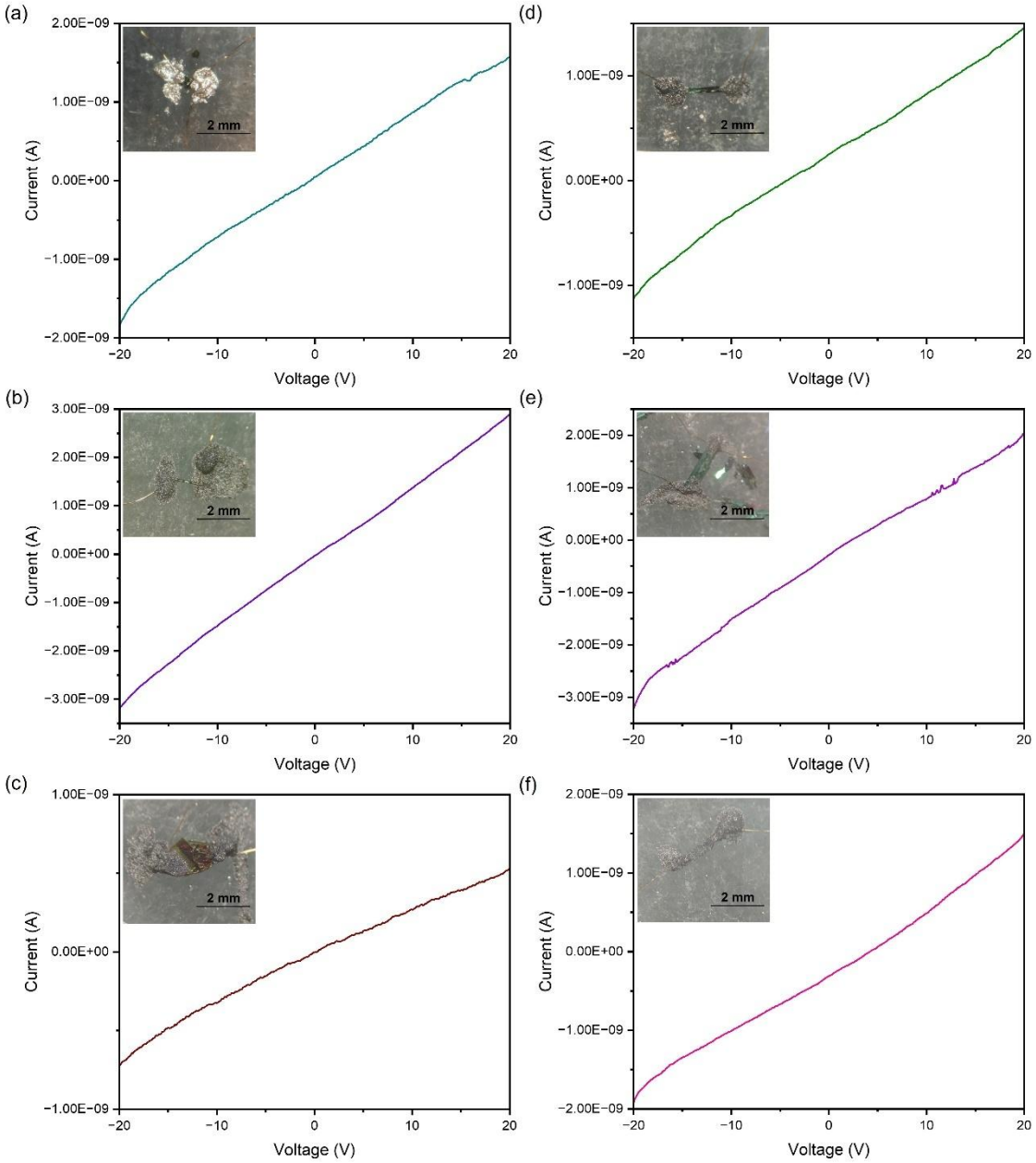

Figure S34. IV curves of **M-1/2**. Insets are corresponding fabricated devices. (a) **Ni-1**, (b) **Pd-1**, (c) **Zn-1**, (d) **Ni-2**, (e) **Pd-2**, (f) **Zn-2**.

Conductivity was calculated according to Equation (3):

$$\sigma = \frac{1}{R}\frac{L}{A} \quad (3)$$

where R, L and A are resistance, length and area respectively.

Table S5. Conductivity of **M-1/2**.

Single crystal	Conductivity(S/m)
Ni-1	$2.6X10^{-7}$
Pd-1	$9.3X10^{-6}$
Zn-1	$1.5X10^{-7}$
Ni-2	$1.2X10^{-6}$
Pd-2	$1.5X10^{-6}$
Zn-2	$7.8X10^{-7}$

9. Computational details

The structures of **Ni-1**, **Ni-2**, **Pd-2**, and **Zn-2** were directly extracted from their respective crystal structures for calculations. The monomeric rhodamine 19 and rhodamine 6G molecules were extracted from the crystal structures of **Ni-1** and **Ni-2**, respectively.

Unless otherwise specified, all density functional theory (DFT) and time-dependent DFT (TDDFT) calculations were performed using Gaussian 16, Revision C.02,[3] with the hybrid functional B3LYP[4] and D3 version of Grimme's dispersion with Becke-Johnson damping.[5,6] For light elements (C, H, N, O, S, Ni, and Zn), the 6-31G* basis set[7,8] was employed. For Pd, scalar relativistic effects were treated using the Stuttgart/Dresden (SDD)[9,10] relativistic effective core potential together with its corresponding valence basis set. All calculations were performed in ACN solvent, modeled using the polarizable continuum model (PCM)[11] with Gaussian 16's default parameters for ACN (dielectric constant ε = 35.688).

The calculated absorption spectra and charge-density difference maps for charge-transfer transitions were generated using Multiwfn 3.8(dev)[12–14] based on TDDFT calculation results. Gaussian broadening with the full width at half maximum (FWHM) of 0.2 eV was applied to the absorption spectra. The density of states (DOS) was generated using Multiwfn by applying Gaussian function broadening to the energies of molecular orbitals (MOs) obtained from DFT calculations, with the FWHM of 0.5 eV. The maps of charge-density difference and MOs were generated using VMD

1.9.3[15]

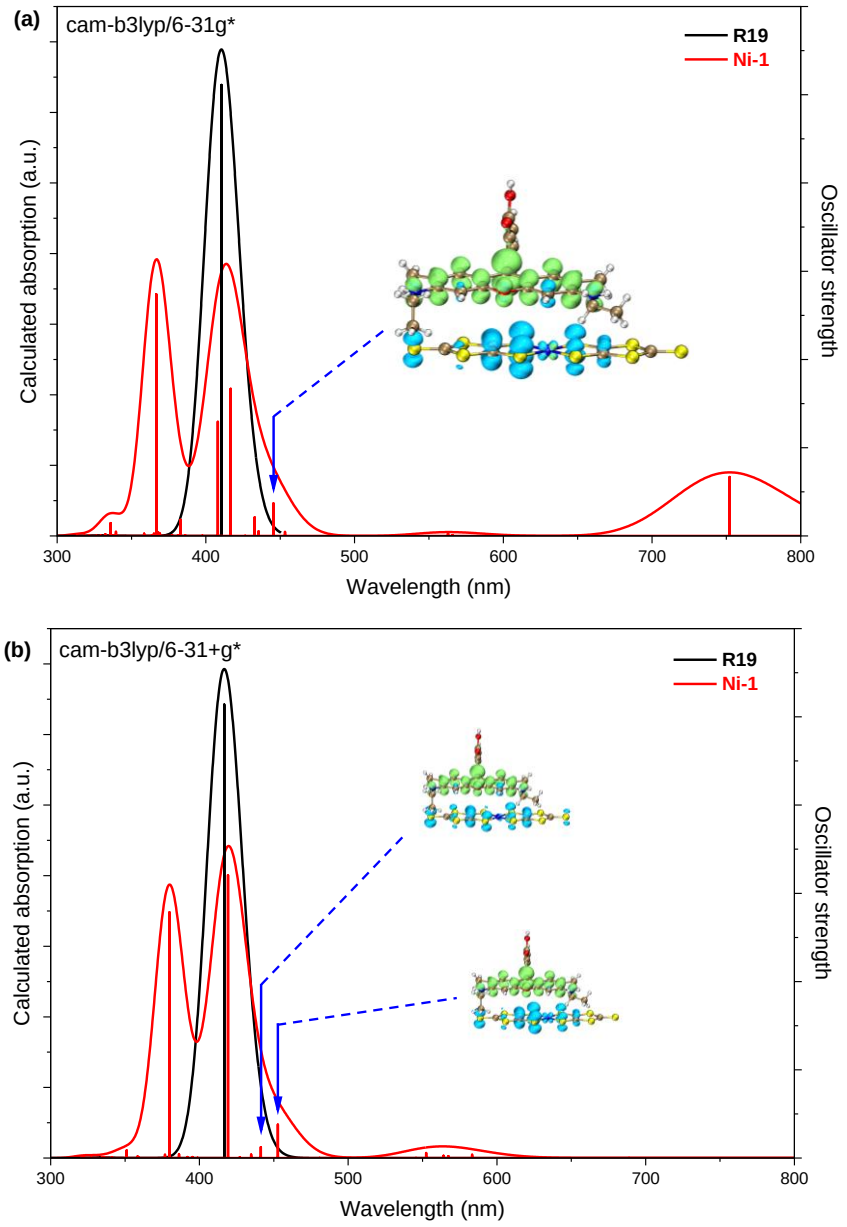

Figure S35. Calculated absorption spectra of **R19** and **Ni-1** (**R19**+**Ni**) at the level of (a) cam-b3lyp/6-31g* and (b) cam-b3lyp/6-31+g*. Inset pictures show charge-transfer transition (isosurface = 0.002 a.u.), with electrons transferring from the blue region to the green region.

References

1 M. Yilmaz, E. Babur, M. Ozdemir, R. L. Gieseking, Y. Dede, U. Tamer, G. C. Schatz, A. Facchetti, H. Usta and G. Demirel, *Nature Mater*, 2017, **16**, 918–924.

2 Z. Zheng, S. Cong, W. Gong, J. Xuan, G. Li, W. Lu, F. Geng and Z. Zhao, *Nat Commun*, 2017, **8**, 1993.

3 Gaussian 16, Revision C.01, M. J. Frisch, G. W. Trucks, H. B. Schlegel, G. E. Scuseria, M. A. Robb, J. R. Cheeseman, G. Scalmani, V. Barone, G. A. Petersson, H. Nakatsuji et.al. Gaussian, Inc., Wallingford CT, 2016.

4 P. J. Stephens, F. J. Devlin, C. F. Chabalowski and M. J. Frisch, *J. Phys. Chem.*, 1994, **98**, 11623–11627.

5 S. Grimme, J. Antony, S. Ehrlich and H. Krieg, *The Journal of Chemical Physics*, 2010, **132**, 154104.

6 S. Grimme, S. Ehrlich and L. Goerigk, *J Comput Chem*, 2011, **32**, 1456–1465.

7 W. J. Hehre, R. Ditchfield and J. A. Pople, *The Journal of Chemical Physics*, 1972, **56**, 2257–2261.

8 P. C. Hariharan and J. A. Pople, *Theoret. Chim. Acta*, 1973, **28**, 213–222.

9 G. Igel-Mann, H. Stoll and H. Preuss, *Molecular Physics*, 1988, **65**, 1321–1328.

10 D. Andrae, U. Häußermann, M. Dolg, H. Stoll and H. Preuss, *Theoret. Chim. Acta*, 1990, **77**, 123–141.

11 G. Scalmani and M. J. Frisch, *The Journal of Chemical Physics*, 2010, **132**, 114110.

12 T. Lu and F. Chen, *J Comput Chem*, 2012, **33**, 580–592.

13 T. Lu, *The Journal of Chemical Physics*, 2024, **161**, 082503.

14 Z. Liu, T. Lu and Q. Chen, *Carbon*, 2020, **165**, 461–467.

15 W. Humphrey, A. Dalke and K. Schulten, *Journal of Molecular Graphics*, 1996, **14**, 33–38.